Article

Melt Composition and Phase Equilibria in the Eclogite-Carbonate System at 6 GPa and 900–1500 °C

Anton Shatskiy [1],*, Altyna Bekhtenova [1], Anton V. Arefiev [1] and Konstantin D. Litasov [2]

[1] Vernadsky Institute of Geochemistry and Analytical Chemistry, Russian Academy of Science, Moscow 119991, Russia

[2] Vereshchagin Institute for High Pressure Physics, Russian Academy of Science, Troitsk, Moscow 108840, Russia

* Correspondence: shatskiyantonf@gmail.com; Tel.: +7-(913)-385-61-29

Abstract: Melting phase relations in the eclogite-carbonate system were studied at 6 GPa and 900–1500 °C. Starting mixtures were prepared by blending natural bimineral eclogite group A (Ecl) with eutectic Na-Ca-Mg-Fe (N2) and K-Ca-Mg-Fe (K4) carbonate mixtures (systems Ecl-N2 and Ecl-K4). In the Ecl-N2 system, the subsolidus assemblage is represented by garnet, omphacite, eitelite, and a minor amount of $Na_2Ca_4(CO_3)_5$. In the Ecl-K4 system, the subsolidus assemblage includes garnet, clinopyroxene, $K_2Mg(CO_3)_2$, and magnesite. The solidus of both systems is located at 950 °C and is controlled by the following melting reaction: $Ca_3Al_2Si_3O_{12}$ (Grt) + 2(Na or K)$_2$Mg(CO$_3$)$_2$ (Eit) = $Ca_2MgSi_3O_{12}$ (Grt) + [2(Na or K)$_2$CO$_3$·CaCO$_3$·MgCO$_3$] (L). The silica content (in wt%) in the melt increases with temperature from < 1 at 950 °C to 3–7 at 1300 °C, and 7–12 at 1500 °C. Thus, no gradual transition from carbonate to kimberlite-like (20–32 wt% SiO_2) carbonate-silicate melt occurs even as temperature increases to mantle adiabat. This supports the hypothesis that the high silica content of kimberlite is the result of decarbonation at low pressure. As temperature increases from 950 to 1500 °C, the melt Ca# ranges from 58–60 to 42–46. The infiltration of such a melt into the peridotite mantle should lower its Ca# and causes refertilization from harzburgite to lherzolite and wehrlitization.

Keywords: carbonate melt; mantle metasomatism; eclogite solidus; mixed paragenesis; Earth's mantle

1. Introduction

Diamondiferous eclogite xenoliths derived from the base of the subcontinental lithospheric mantle (SCLM) often show traces of mantle metasomatism [1–4]. Three-dimensional, high-resolution X-ray computed tomography of eclogite xenoliths has revealed that diamonds grew in metasomatic alteration zones [5–7]. Numerous microinclusions of calcite and alkaline Cl-bearing carbonate melt found in diamonds from metasomatic veins in eclogite xenoliths [1,8,9] indicate that diamonds were formed during percolation of a carbonatitic melt through eclogite.

Mantle carbonatitic melts entrapped by diamonds from kimberlites and placers worldwide are rich in alkalis. Based on over a hundred analyses of carbonatitic inclusions containing <15 wt% SiO_2 and ≤5 Cl wt% [10–21], the mantle carbonatitic melts contain (average/maximum) 6/19 wt% Na_2O and 12/75 wt% K_2O (see Supplementary Table S7 [22]). An affinity of high- and low-Mg carbonatitic melts to diamonds of peridotitic and eclogitic suits, respectively, was also revealed [23]. Moreover, inclusions intermediate between low-Mg carbonatitic and saline melts have been found in diamonds recovered from a xenolith of bimineralic eclogite Group B [8,13].

Alkali-rich carbonatitic inclusions have also been found in sheared garnet and spinel peridotite xenoliths derived from 110–230 km depths and magmatic minerals from kimberlites of Siberia, Canada, Greenland, and Africa [24–35]. Interestingly, alkaline carbonatite

inclusions have been found in sheared peridotite xenoliths [30,32–35], while no such inclusions have been reported to occur in granular peridotite xenoliths. The latter was explained by the segregation of carbonatite melt in zones of intense deformation, by means of a dissolution–precipitation mechanism driven by mechanical stress [36].

Although the compositions of alkaline carbonate melts in equilibrium with peridotites under P-T conditions of the subcontinental lithospheric mantle and underlying asthenosphere were recently reported [37,38], data on the temperature stability range and compositions of carbonate melts equilibrium with eclogite in the mantle are rather contradictory. Estimates of the temperatures of carbonated eclogite solidus vary from ~1000 to 1350 °C at 5–6 GPa [39–44]. The experimental data on the composition of carbonate melts in equilibrium with eclogites are very limited and scattered. The reliability of a few available data points is questionable. A study of the melt compositions in experiments on the melting of the carbonated eclogites showed that these compositions do not undergo complete melting at the specified P-T conditions [45,46]. The results also showed that the stable melts have an alkaline carbonate composition similar to the eutectic melts in the Na_2CO_3-$CaCO_3$-$MgCO_3$ and K_2CO_3-$CaCO_3$-$MgCO_3$ systems at 6 GPa [47–50].

Given that alkaline carbonate melts are responsible for mantle metasomatism and diamond formation [8,51–53], it is interesting to know their compositions in equilibrium with eclogites at the base of SCLM and the underlying asthenosphere.

We have recently shown that such melts can be in equilibrium with eclogite at 1100 and 1200 °C at 6 GPa [54]. However, the temperature range, expected for the operation of metasomatizing carbonate melts in the mantle, is much wider. The temperature estimates for the formation of metasomatized and diamond-bearing eclogitic xenoliths and touching garnet-omphacite inclusions in diamonds fall in the range of 900–1500 °C [3,55]. The homogenization temperature of some carbonate-bearing microinclusions in cuboid diamonds reaches the temperature of the convective mantle [56], 1400–1500 °C [57].

Here, we present new experimental data on the solidus, melting reactions, and trends in the compositions of carbonate melts in the systems consisting of natural eclogite + Na-Ca-Mg-Fe and K-Ca-Mg-Fe carbonate mixtures over 900–1500 °C at 6 GPa.

2. Methods

2.1. Starting Materials

Starting materials were prepared by blending synthetic carbonate mixtures and powder of natural eclogite. The compositions of starting materials are given in Tables 1 and S1–S3.

Table 1. Composition (wt%) of starting materials.

Component	SiO₂	TiO₂	Al₂O₃	Cr₂O₃	NiO	FeO	MnO	MgO	CaO	Na₂O	K₂O	CO₂
Ecl UD-45-02	46.1	0.30	15.2	0.43	0.00	8.45	0.33	17.68	10.6	0.60	0.34	–
Cpx	55.1	0.18	2.01	0.23	b.d.l.	4.11	0.10	16.2	20.3	1.70	0.03	–
Grt	41.7	0.32	22.2	0.38	b.d.l.	10.8	0.38	18.6	5.60	0.08	b.d.l.	–
N2	–	–	–	–	–	2.38	0.03	4.71	20.3	29.3	–	43.3
K4	–	–	–	–	–	2.72	0.03	5.39	21.2	–	31.7	39.0
Ecl-N2	29.3	0.19	9.61	0.28	0.00	6.23	0.22	12.9	14.1	11.1	0.22	15.8
Ecl-K4	28.1	0.19	9.23	0.26	0.00	6.21	0.21	12.9	14.7	0.37	12.6	15.2

Fresh xenolith of bimineral eclogite (UD-45-02) from the Udachnaya kimberlite pipe (Yakutia, Russia) [58], similar to that used in our previous study [54], was employed. The xenolith was chosen because it does not contain visible traces of secondary alterations and undoubtedly is of mantle origin. Compositions of clinopyroxene, $Di_{78}Jd_{12}En_4Fs_6$, and garnet, $Prp_{65}Alm_{21}Grs_{14}$, correspond to Group A eclogite according to the classifications of Taylor and Neal [59] and Coleman, et al. [60], respectively (Table 1). Mass balance calculations indicate that the xenolith consists of 65 wt% garnet and 35 wt% clinopyroxene (Table S1). Although the eclogite does not contain phlogopite, the IR spectra of omphacite

and garnet revealed the presence of a minor amount of water as hydroxyl structural defects. Considering the volume ratios of minerals, the bulk water content in the xenolith is estimated to be 576 ppm H_2O [58]. Assuming a pressure of 5 GPa, the geothermometer of Ellis and Green [61] gives a temperature of 1193 °C [58]. It was also recently found that the xenolith UD-45-02 contains diamonds (V.S. Shatsky personal communication). Representative pieces of xenolith were ground with alcohol in a tungsten carbide mortar.

The starting carbonate mixtures, N2 and K4, were close to eutectics established at 6 GPa and 1050 °C in the Na_2CO_3-$CaCO_3$-$MgCO_3$ and K_2CO_3-$CaCO_3$-$MgCO_3$ systems, respectively [49,50]. The mixtures were blended from reagent grade Na_2CO_3, K_2CO_3, $CaCO_3$, natural magnesite (<0.1% impurity) from Brumado (Bahia, Brazil), and siderite, $Fe_{0.83}Mn_{0.01}Mg_{0.08}Ca_{0.08}CO_3$, from Farmsen Clay Pit, Schellerten, Hildesheim (Lower Saxony, Germany) (Table 1 and S2). The iron number, Fe# = $100 \cdot Fe/(Fe + Mg)$, of carbonate mixtures, 22 mol%, was close to that of eclogite UD-45-02, 21 mol%.

The eclogite powder and carbonate mixtures were ground under acetone in a tungsten carbide mortar. The carbonate/silicate ratio in each starting material was 40/60 in mol%, which corresponds to a bulk CO_2 content of 20 mol% or 15–16 wt% (Table 1 and S3).

2.2. High-Pressure Experiments

Since the starting mixtures contain hygroscopic compounds, K_2CO_3 and Na_2CO_3, special care was applied to prevent samples' contamination with atmospheric water. The prepared assemblies with loaded samples were dried at 200 °C for ≥12 h under vacuum prior to experiment. To minimize the contamination of the dried cell with water during its loading into the press, indoor humidity was maintained at 15%–35%.

The design of the cell assembly is identical to that used by Shatskiy et al. [62]. The assembly includes an octahedral pressure medium made of ZrO_2 ceramics [63], a graphite heater with 4.0/4.5 mm inner/outer diameter, and a W/Re (3%/25%) thermocouple, electrically insulated by Al_2O_3 tubes. The powdered samples were loaded in graphite capsules, electrically insulated from the heater by a thin (0.2 mm) MgO-SiO2 ceramic sleeve.

Eight tungsten carbide cubes ("Fujilloy N-05") of 26 mm in size with 12-mm truncations were used as anvils to compress the octahedral cell assembly. Pyrophyllite gaskets, 4.0 mm in width and thickness, were fixed by rice glue at the edges of truncations to support anvil flanks. The experiments were run on a 1500-ton multianvil DIA-type press 'Discoverer'.

The temperature gradients in the cell were examined using thermal modelling software [64]. The results revealed that the temperature gradient within individual samples varies from 7 to 14 °C/mm. The correctness of the modelling was verified experimentally [65] using the two-pyroxene thermometer [66].

Experiments were performed by 4-h compression to a load of 6.5 MN, corresponding to a sample pressure of 6 GPa, and heating to a target temperature at a rate of 25–50 °C/min. Then samples were annealed for 198 h at 900 °C, 168 h at 950 °C, 169 h at 1000 °C, 64 h at 1300 °C, 24 h at 1400 °C, and 5 h at 1500 °C. During annealing, the temperature was maintained within 2–3 °C of the desired value at a constant press load. The experiments were terminated by turning off the heater power, resulting in a temperature drop below 150 °C in a few seconds, followed by 5-h decompression.

2.3. Analytical Techniques

Immediately after experiments, the recovered graphite cassettes with samples were filled with epoxy under vacuum. Then capsules were sliced using a low-speed diamond saw to recover nearly axial, vertical cross-sections of samples. The obtained specimens were placed on a double-sided tape in a plexiglass holder with epoxy. The samples were then polished under oil using 400(37)-, 1000(13)-, and 1500(9)-mesh (µm) sandpapers. Finally, samples were polished using a 3 µm diamond paste. After polishing, the samples were cleaned using petroleum benzine and wipes and then stored in benzine before carbon coating.

Samples were studied using a MIRA 3 LMU scanning electron microscope (Tescan Orsay Holding, Brno-Kohoutovice, Czech Republic), coupled with an INCA energy-dispersive X-ray microanalysis system 450, equipped with liquid nitrogen-free Large area EDX X-Max-80 Silicon Drift Detector (Oxford Instruments Nanoanalysis Ltd., High Wycombe, UK) [67]. Energy-dispersive X-ray spectra (EDS) were collected by using an electron beam-rastering method, in which the stage was stationary while the electron beam moved over the surface area, with dimensions 5–30 μm (for silicate minerals) and 50–500 μm (for quenched melt) at 20 kV accelerating voltage and 1.5 nA beam current. The live counting time for X-ray spectra was 20 s. The silicon drift detector energy-dispersive X-ray spectrometry (SDD-EDS) enables accuracy and precision equivalent to that of wavelength-dispersive spectroscopy in the case of routine analysis of rock-forming silicate minerals [67,68] and even shows better performance in the case of alkali-rich carbonate samples, which are unstable (i.e., decompose and evaporate) under the strong stationary electron beam [69].

3. Results

The symbols used in the manuscript are given in the abbreviations section.

3.1. Textures of Recovered Samples

Representative backscattered electron (BSE) images of the samples are shown in Figures 1 and 2. Below the solidus, at 900 °C, the crystalline phases are homogeneously distributed throughout the sample (Figure 1a,b). At 950 °C, the sample consists of the subsolidus assemblage in the low-temperature (LT) zone and quenched melt with suspended clinopyroxene and garnet crystals in the high-temperature (HT) zone (Figures 1c–e and 2a,b). Above the solidus over 1000–1500 °C, the melt forms a separate pool in the HT sample side, while an aggregate of clinopyroxene and garnet crystals adjoins the LT side (Figures 1c–l and 2c,e). The carbonate melt quenches to an aggregate of needle-shaped carbonate crystals up to 60 μm in length (Figure 1d). At 1500 °C, needle-shaped clinopyroxene crystals appear in addition to carbonate (Figures 1l and 2f).

Clinopyroxene, garnet, and olivine form euhedral to subhedral grains 5–50 μm in size (Figures 1 and 2). Relicts with the initial composition remain in the larger garnet crystals, while the smaller ones are free of relicts (Figure 1b). In the Ecl-N2 system over 1100–1300 °C, in addition to clinopyroxene and garnet, a minor amount of olivine appears as well-shaped euhedral crystals up to 15 μm in size (Figure 1i).

Carbonates (eitelite, magnesite, $Na_2Ca_4(CO_3)_5$, and $K_2Mg(CO_3)_2$) are present over 900–950 °C between silicate minerals (Figures 1a–e and 2b). Magnesite crystals are also present at 1000 °C adjacent to the LT capsule end (Figure 1g).

3.2. Phase Relations

Successive changes in the phase assemblage with increasing temperature are shown in Figure 3. The run conditions and the modal abundance of phases are listed in Tables 2 and S1–S10 both in mol% and wt%. The mass balance calculations are given in Tables S5 and S6 in mol% and wt%, respectively.

The system Ecl-N2. At 900 °C (run D280, 198 h), the sample is represented by the subsolidus assemblage consisting of clinopyroxene, garnet, eitelite, and a trace amount of $Na_2Ca_4(CO_3)_5$ (Figure 1a,b, Table 2). As the temperature increases to 950 °C (run D267, 168 h), melting begins, $Na_2Ca_4(CO_3)_5$ disappears, while eitelite is still present (Figure 1c–e, Table 2).

At 1000 °C (run D253, 169 h), eitelite disappears, while a minor amount of magnesite (3 wt%) is present (Figure 1f,g, Figure 3a and Table 2). At 1300 °C (run D211, 64 h), a minor amount of olivine (1 wt%) appears in addition to clinopyroxene and garnet similar to that observed at 1100 and 1200 °C in our earlier study [54] (Figure 1h,i, Figure 3a and Table 2). At 1400 °C (run D214, 24 h) and 1500 °C (run D217, 5 h), olivine disappears, the clinopyroxene fraction slightly decreases, and the melt fraction increases (Figure 3a).
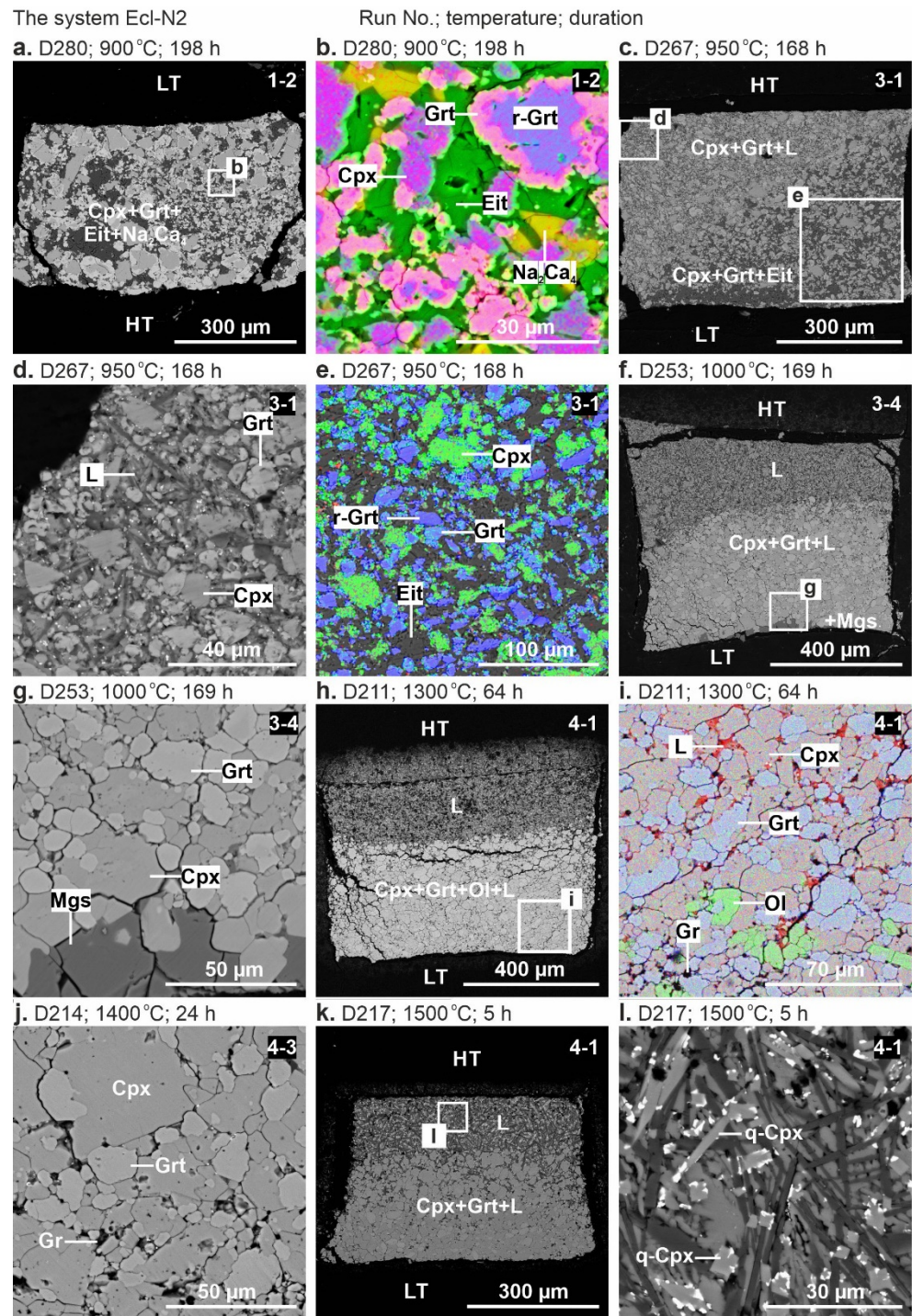
Figure 1. BSE images of sample cross-sections from 6-GPa experiments in the system Ecl-N2 at 900 °C (**a,b**), 950 °C (**c–e**), 1000 °C (**f,g**), 1300 °C (**h,i**), 1400 °C (**j**), and 1500 °C (**k,l**). HT—high-temperature and LT—low-temperature sample sides. The gravity vector is directed downward. The color images (**b,e,i**) were taken in the element mapping mode. The numbers at the top-right corners of each subfigure are sample numbers. See the abbreviations section for mineral and phase symbols.
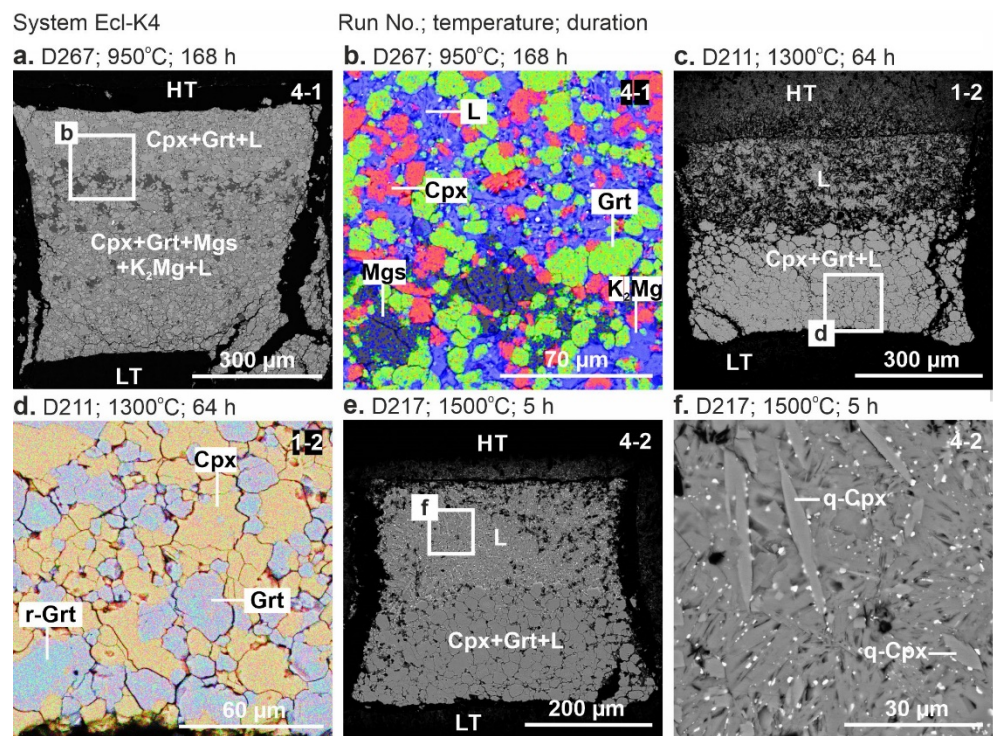
Figure 2. BSE images of sample cross-sections from 6-GPa experiments in the systems Ecl-K4 at 950 °C (**a**,**b**), 1300 °C (**c**,**d**), 1500 °C (**e**,**f**). See the Figure 1 caption for other details. See the abbreviations section for mineral and phase symbols.
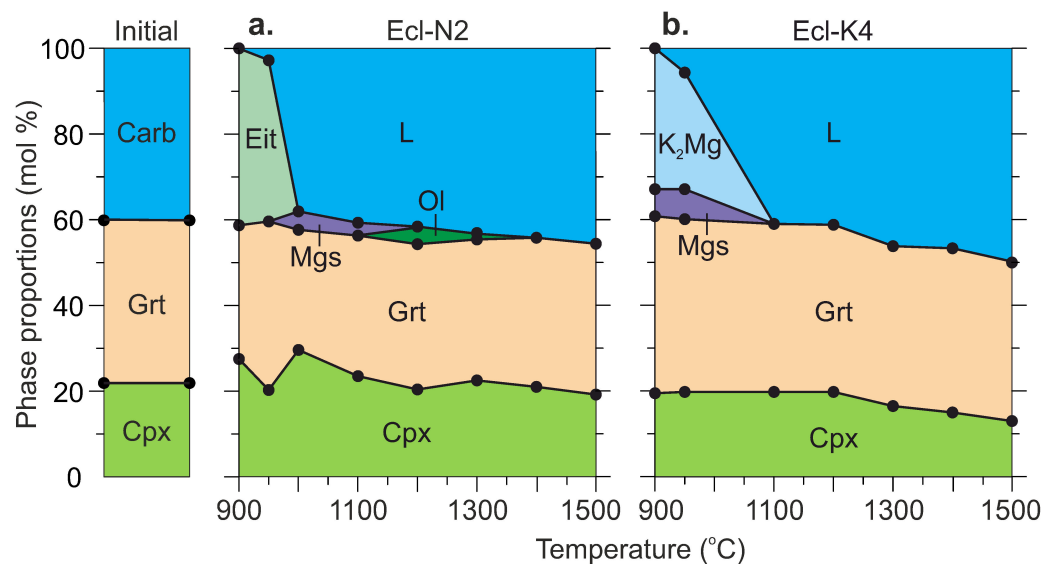

Figure 3. Modal abundances of phases as a function of temperature in the systems Ecl-N2 (**a**) and Ecl-K4 (**b**) at 6 GPa. Modes (in mol%) were determined from the bulk compositions of starting mixtures and compositions of phases measured by EDS (Table S5). Modes in wt% are given in Table S6. See the abbreviations section for mineral and phase symbols. The data at 1100 and 1200 °C are after [54]. See the abbreviations section for mineral and phase symbols.

Table 2. Modal abundance of phases (in wt%) in the experimental samples.

| System Run | T, °C | t, h | Run Products | | | | | | | | |
			Cpx	Grt	Ol	Na₂Ca₄	Eit	K₂Mg	Mgs	L	Sum r²
Ecl-N2	Initial mixture		22	41	–	–	–	–	–	37	
D280	900	198	25	40	–	tr.	35	–	–	–	4.00
D267	950	168	21	45	–	–	32	–	–	2	0.15
D253	1000	169	31	31	–	–	–	–	–	35	1.98
D178 *	1100	111	23	37	3	–	–	–	tr.	37	0.06
D178S *	1100	111	28	32	1	–	–	–	–	38	0.56
D174 *	1200	86	21	38	5	–	–	–	–	37	1.53
D174S *	1200	86	21	39	3	–	–	–	–	37	1.73
D211	1300	64	23	37	1	–	–	–	–	39	0.43
D214	1400	24	23	37	–	–	–	–	–	40	0.35
D217	1500	5	21	36	–	–	–	–	–	43	0.80
Ecl-K4	Initial mixture		21	40	–	–	–	–	–	39	
D280	900	198	19	42	–	–	–	33	6	–	0.68
D267	950	168	19	44	–	–	–	4	28	5	0.18
D178 *	1100	111	18	42						40	2.30
D178S *	1100	111	19	41	–	–	–	–	–	40	1.51
D174 *	1200	86	19	41	–	–	–	–	–	40	1.72
D174S *	1200	86	17	43	–	–	–	–	–	40	2.32
D211	1300	64	17	38	–	–	–	–	–	45	0.28
D214	1400	24	15	40	–	–	–	–	–	45	0.88
D217	1500	5	13	39	–	–	–	–	–	48	3.79

Notes: *t*—run duration. Weight fraction of phase estimated from mass balance calculations. The calculations and standard deviations are given in Tables S4–S6 both in mol% and wt%. tr.—trace amount. *—after [54]. S—synthetic mixture instead of the rock. "Sum r²" is the summation of squares of residuals obtained by using mineral modes, phase compositions, and composition of the starting materials. See the abbreviations section for mineral and phase symbols.

The system Ecl-K4. At 900 °C (run D280, 198 h), the sample consists of clinopyroxene, garnet, K₂Mg(CO₃)₂, and magnesite (Figure 3b, Table 2). At 950 °C (run D267, 168 h), the resulting mineral assemblage remains unchanged, while the melt fraction increases at the expense of K₂Mg(CO₃)₂ (Figures 2c,d and 3b). Over 1300–1500 °C (runs D211, D214, D217), the samples are represented by clinopyroxene, garnet, and quenched melt (Figures 2e–h and 3b) as that observed by Shatskiy et al. [54] in the same system at 1100 and 1200 °C (Figure 3b, Table 2).

3.3. Composition of Phases

The chemical composition of phases is given in Table 3 in wt% and Tables S1–S10 both in mol% and wt%.

Table 3. Phase compositions in wt%, normalized to 100%.

System, T, °C, Run No., Duration	Phase	n	SiO₂	TiO₂	Al₂O₃	Cr₂O₃	FeO	MnO	MgO	CaO	Na₂O	K₂O	CO₂ *	Ca #
Ecl UD-42-02	Cpx		55.1	0.18	2.01	0.23	4.11	0.10	16.2	20.3	1.70	0.03	–	44
Ecl-N2	Grt		41.7	0.32	22.2	0.38	10.8	0.38	18.6	5.60	0.08	b.d.l.	–	14
900, D280, 198 h	Cpx	4	54.6 (1.3)	b.d.l.	5.08 (39)	0.11 (5)	4.42 (12)	b.d.l.	13.0 (1.0)	18.5 (5)	4.26 (75)	b.d.l.	–	46
	Grt	9	38.9 (4)	0.39 (6)	19.2 (5)	0.43 (4)	12.0 (7)	0.32 (6)	4.33 (61)	24.0 (4)	0.30 (17)	b.d.l.	–	61
	Na₂Mg	9	–	–	–	–	2.10 (6)	b.d.l.	21.3 (8)	1.29 (15)	28.6 (1.1)	0.52 (1)	46.1 (1.6)	4
	Na₂Ca₄	2	–	–	–	–	1.36	b.d.l.	2.32	40.6	11.9	0.09	43.7	90
950, D267, 168 h	Cpx	3	54.8 (6)	0.05 (6)	4.82 (33)	0.22 (2)	3.89 (30)	b.d.l.	13.8 (1.0)	18.9 (4)	3.43 (41)	b.d.l.	–	46
	Grt	9	39.9 (2)	0.61 (7)	19.4 (3)	0.49 (3)	10.3 (3)	0.38 (3)	7.48 (1.46)	21.2 (2.1)	0.32 (13)	b.d.l.	–	53

Table 3. *Cont.*

System, T, °C, Run No., Duration	Phase	n	SiO₂	TiO₂	Al₂O₃	Cr₂O₃	FeO	MnO	MgO	CaO	Na₂O	K₂O	CO₂ *	Ca #
	Na₂Mg	3	–	–	–	–	1.74 (5)	b.d.l.	20.9 (8)	1.43 (1)	29.5 (1.0)	0.31 (2)	46.1 (1.7)	4
	L	9	0.62 (15)	0.13 (6)	0.42 (48)	b.d.l.	3.43 (59)	b.d.l.	8.31 (1.75)	19.8 (2.5)	23.2 (1.8)	1.05 (33)	43.0 (2.7)	58
1000, D253, 169 h	Cpx	22	55.9 (8)	0.23 (6)	8.86 (76)	0.35 (3)	2.68 (20)	b.d.l.	11.0 (1.1)	15.2 (1.0)	5.79 (65)	b.d.l.	–	47
	Grt	7	40.9 (2)	0.30 (4)	22.0 (8)	0.42 (3)	11.4 (1)	0.42 (2)	14.1 (7)	10.3 (8)	b.d.l.	b.d.l.	–	26
	Mgs	4	–	–	–	–	7.59 (2)	b.d.l.	40.0 (3)	2.25 (24)	b.d.l.	b.d.l.	50.1 (3)	4
	L	6	1.10 (25)	0.17 (6)	0.27 (4)	b.d.l.	4.67 (14)	b.d.l.	9.12 (26)	16.6 (2)	25.0 (3)	0.26 (1)	42.8 (7)	50
1300, D211, 64 h	Cpx	18	54.7 (4)	0.15 (6)	6.54 (60)	0.21 (5)	3.45 (11)	b.d.l.	13.1 (9)	17.9 (6)	3.89 (43)	b.d.l.	–	46
	Grt	10	41.3 (5)	0.50 (4)	21.1 (4)	0.62 (4)	9.83 (89)	0.37 (6)	15.2 (1.7)	10.8 (2.5)	0.22 (19)	b.d.l.	–	27
	Ol	1	40.2	b.d.l.	b.d.l.	b.d.l.	13.8	b.d.l.	45.8	0.2	b.d.l.	b.d.l.	–	0
	L	5	2.77 (9)	b.d.l.	0.20 (4)	b.d.l.	4.83 (4)	b.d.l.	9.66 (19)	15.7 (3)	24.8 (2)	0.51 (2)	41.5 (4)	48
1400, D214, 24 h	Cpx	20	54.5 (4)	b.d.l.	6.90 (48)	0.25 (4)	3.45 (13)	b.d.l.	13.3 (5)	17.7 (7)	3.82 (31)	b.d.l.	b.d.l.	45
	Grt	5	41.1 (7)	0.43 (4)	21.6 (4)	0.58 (2)	8.98 (75)	0.37 (9)	15.5 (1.0)	11.3 (1.3)	0.16 (14)	b.d.l.	b.d.l.	28
	L	8	4.44 (29)	0.08 (6)	0.28 (6)	b.d.l.	5.33 (12)	b.d.l.	9.69 (74)	15.2 (8)	24.2 (9)	0.75 (3)	40.0 (2.2)	46
1500, D217, 5 h	Cpx	8	54.5 (3)	b.d.l.	8.35 (25)	0.34 (3)	3.01 (12)	b.d.l.	12.7 (3)	16.8 (4)	4.36 (19)	b.d.l.	–	46
	Grt	6	41.5 (2)	0.34 (6)	21.8 (1)	0.55 (3)	8.17 (91)	0.33 (7)	16.1 (6)	11.0 (1.4)	0.19 (12)	b.d.l.	–	28
	L	3	7.06 (1.18)	0.06 (0)	0.62 (12)	b.d.l.	5.55 (25)	0.13 (9)	9.42 (13)	15.0 (2)	23.2 (6)	1.72 (2)	37.3 (8)	46
	q-Cpx	1	51.4	1.17	5.05	0.04	7.71	0.12	15.1	15.7	3.63	0.08	–	37
Ecl-K4														
900, D280, 198 h	Cpx	3	55.0 (0)	0.15 (0)	1.65 (5)	0.12 (4)	2.98 (29)	b.d.l.	16.5 (1)	22.2 (6)	1.03 (11)	0.33 (2)	–	47
	Grt	14	39.8 (4)	0.53 (8)	20.0 (3)	0.53 (7)	10.7 (2)	0.42 (5)	6.84 (59)	21.1 (9)	b.d.l.	b.d.l.	–	54
	K₂Mg	6	–	–	–	–	2.53 (2)	b.d.l.	15.6 (8)	1.96 (18)	0.65 (18)	39.9 (3)	39.3 (1.2)	8
	Mgs	9	–	–	–	–	8.02 (15)	0.15 (4)	39.7 (1.5)	2.15 (29)	b.d.l.	b.d.l.	50.0 (1.5)	3
950, D267, 168 h	Cpx	11	54.8 (5)	b.d.l.	1.55 (23)	b.d.l.	2.62 (54)	b.d.l.	16.8 (4)	22.8 (1.5)	0.84 (42)	0.47 (15)	–	47
	Grt	20	40.0 (3)	0.46 (6)	20.0 (3)	0.50 (5)	10.7 (3)	0.37 (5)	8.24 (95)	19.7 (1.4)	b.d.l.	b.d.l.	–	49
	K₂Mg	6	–	–	–	–	2.59 (13)	b.d.l.	15.2 (1.4)	2.91 (27)	0.57 (0)	39.5 (0)	39.3 (1.2)	11
	Mgs	7	–	–	–	–	7.54 (12)	0.15 (5)	39.4 (1.2)	2.93 (20)	b.d.l.	b.d.l.	50.0 (1.8)	5
1300, D211, 64 h	L	2	1.08	b.d.l.	0.28	b.d.l.	4.38	b.d.l.	7.00	19.5	1.16	28.0	38.6	60
	Cpx	2	54.2	b.d.l.	2.64	b.d.l.	3.32	b.d.l.	16.6	22.3	0.74	0.29	–	47
	Grt	2	41.2	0.20	22.0	0.61 (1)	8.27	0.27	15.2	12.3	b.d.l.	b.d.l.	–	31
1400, D214, 24 h	L	4	6.92 (1.03)	0.10 (9)	0.90 (13)	b.d.l.	5.35 (16)	b.d.l.	9.25 (99)	14.7 (1.4)	0.89 (17)	28.4 (1.7)	33.4 (2.4)	46
	Cpx	2	54.0	b.d.l.	2.07	b.d.l.	3.04	0.09	16.9	22.9	0.47	0.44	–	47
	Grt	2	41.6	0.21	21.8	0.46	7.59	0.26	15.5	12.6	b.d.l.	b.d.l.	–	31
1500, D217, 5 h	L	6	7.67 (1.55)	0.20 (8)	0.78 (12)	b.d.l.	5.70 (35)	b.d.l.	8.80 (1.10)	14.0 (1.8)	1.12 (10)	29.2 (1.2)	32.5 (1.7)	46
	Cpx	7	54.1 (4)	b.d.l.	2.39 (19)	b.d.l.	3.01 (14)	b.d.l.	16.9 (4)	22.5 (2)	0.53 (14)	0.45 (6)	–	47
	Grt	8	41.8 (2)	0.14 (9)	21.7 (1)	0.56 (5)	6.62 (33)	0.23 (9)	15.5 (4)	13.4 (8)	b.d.l.	b.d.l.	–	33
	L	9	12.2 (1.5)	0.20 (9)	1.15 (10)	b.d.l.	5.83 (28)	b.d.l.	9.51 (69)	13.1 (6)	1.03 (18)	28.2 (8)	28.7 (6)	42
	q-Cpx	1	50.1	0.73	4.68	b.d.l.	6.53	0.12	15.5	19.1	1.21	1.94	–	42

Notes: b.d.l.—below detection limit; n—number of measurements; standard deviation is given in brackets; CO₂ *—CO₂ abundance in carbonate phases calculated as CO₂ = FeO + MnO + MgO + CaO + Na₂O + K₂O–SiO₂–Al₂O₃, assuming all CO₂ in the liquids in carbonate ion form; Ca# = 100·Ca/(Ca + Mg); q-Cpx – clinopyroxene form the melt quench products. See the abbreviations section for mineral and phase symbols.

3.3.1. Clinopyroxene

Equilibration with the Na-rich carbonate melt (N2) increases Na₂O in clinopyroxene from the initial 1.7 to 5.8 wt% (Tables 1, 3 and S8). In contrast, equilibration with the K-rich carbonate melt (K4) decreases Na₂O from 1.7 to 0.3 wt% and increases K₂O

from the initial 0.03 to 0.6 wt% (Tables 1, 3 and S8). Thus, after the experiments, the clinopyroxenes in Ecl-N2, belong to Group B eclogites, according to the classification of Taylor and Neal [59], whereas those in Ecl-K4 belong to Group A eclogites or garnet clinopyroxenes (Figure 4). Like the equilibrium clinopyroxene, the one in the melt quench products (q-Cpx) recovered from 1500 °C is almost free of K_2O and contains 3.6 wt% Na_2O in the Ecl-N2 system, while in the Ecl-K4 system, q-Cpx contains 1.2 wt% Na_2O and 1.9 wt% K_2O (Tables 3 and S8). In both systems, q-Cpx is richer in FeO (6.5–7.7 wt%) and TiO_2 (0.7–1.2 wt%) than the initial and equilibrium clinopyroxene (Tables 1, 3 and S8).
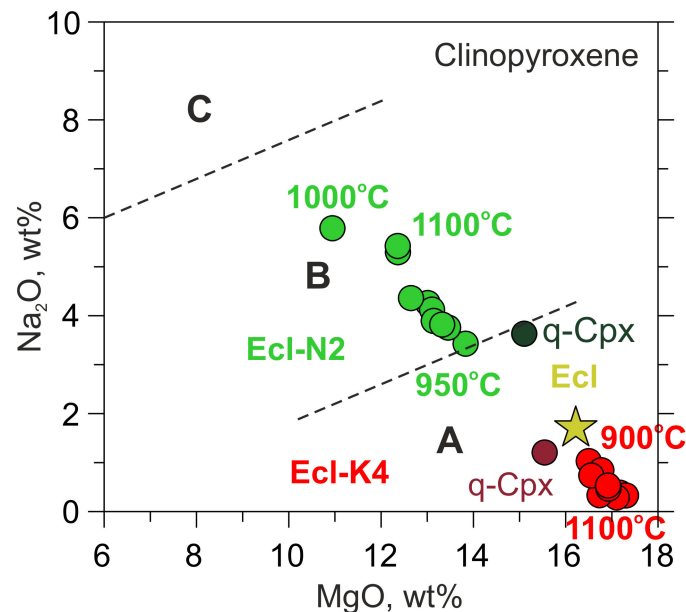
Figure 4. Na_2O vs. MgO in clinopyroxenes from 6-GPa experiments in the systems Ecl-N2 (green) and Ecl-K4 (red). q-Cpx clinopyroxene from the melt quench products. Clinopyroxene from the original eclogite is denoted by a yellow star. Group A, B, and C according to the classification of Taylor and Neal [59]. The data at 1100 and 1200 °C are after [54].

3.3.2. Olivine

Olivine is a minor phase at 1300 °C in the Ecl-N2 system (Figure 3b). It has $Fo_{86}Fa_{14}$ composition and contains 0.3 wt% CaO (Table 3 and Table S10).

3.3.3. Carbonates

At 900–950 °C, eitelite, $(Na_{0.99}K_{0.01})_2(Mg_{0.91}Fe_{0.05}Ca_{0.04})(CO_3)_2$, and $(K_{0.98}Na_{0.02})_2$ $(Mg_{0.84}Fe_{0.08}Ca_{0.08})(CO_3)_2$ crystallize in the Ecl-N2 and Ecl-K4 systems, respectively (Figure 3, Tables 3 and S11). Magnesite with approximate composition, $(Mg_{0.87}Fe_{0.09}Ca_{0.04})$ CO_3, is a minor phase in both systems (Figure 3, Tables 3 and S4).

3.3.4. Melt

The melt has an alkali-rich carbonate composition (Tables 3 and S7). At 900–950 °C, the melt has Ca# 58–60 and coexists with Mg-rich carbonates, eitelite in the Ecl-N2 system and $K_2Mg(CO_3)_2$ + magnesite in the Ecl-K4 system (Figure 6b, Table 3). As temperature increases to 1100 °C, the melt consumes Mg-carbonates and its Ca# decreases to 47–54 (Figure 6b, Tables 3 and S7). The silica content in the melt increases from <1 wt% over 900–950 °C to 3–7 wt% at 1300 °C, and 7–12 wt% at 1500 °C (Figure 6a, Tables 3 and S7). The alumina content in the melt also increases with temperature but does not exceed 1.2 wt% (Table 3). Over 1300–1500 °C, the silica content in the K-rich melt is about two times higher than that in the Na-rich melt (Figure 6b, Tables 3 and S7). An increase in the silica concentration in the melt is accompanied by a decrease in the clinopyroxene fraction.

This is especially evident in the Ecl-K4 system (Figure 3, Table 2). Unlike clinopyroxene, the fraction of garnet remains unchanged. Thus, garnet is buffering the low Al_2O_3 in the melt.
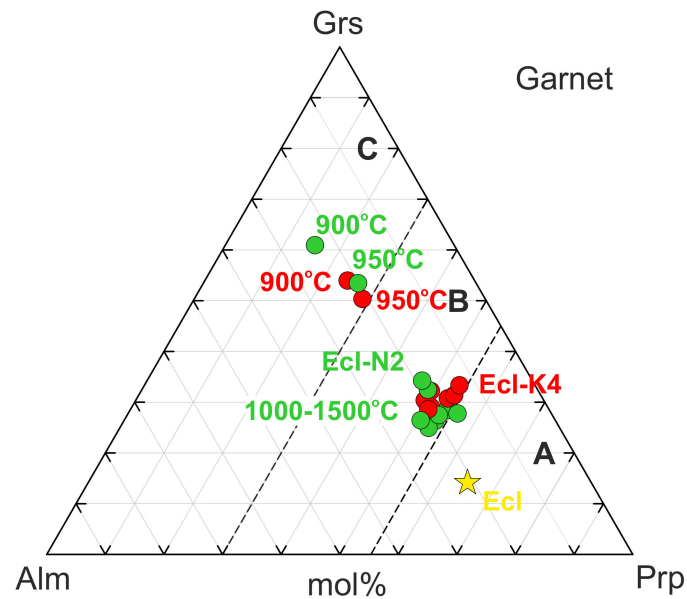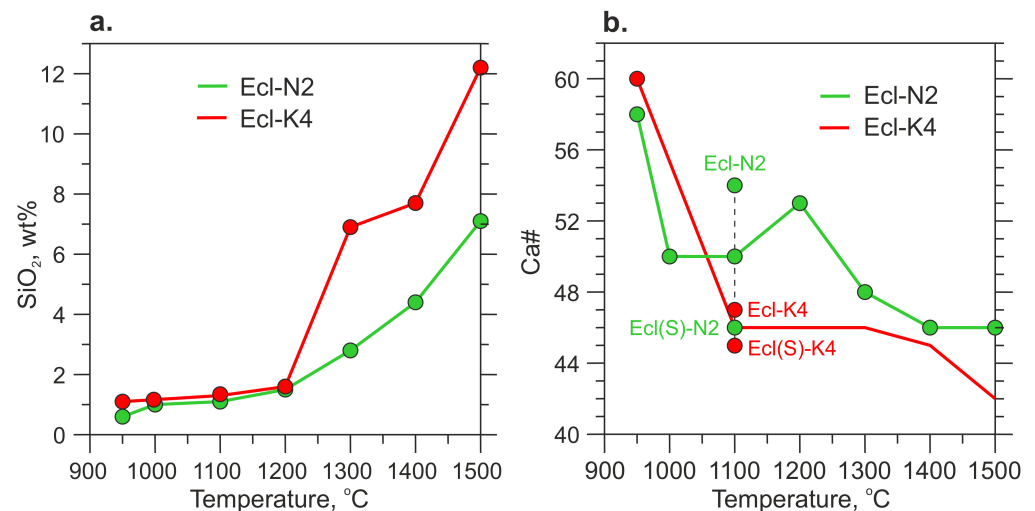

Figure 5. Garnet compositions from 6-GPa experiments in the systems Ecl-N2 (green) and Ecl-K4 (red) expressed in terms of grossular–pyrope–almandine. Garnet from the original eclogite is denoted by a yellow star. Group A, B, and C according to the classification of Coleman et al. [60].

Figure 6. Silica content (**a**) and Ca# (**b**) in the carbonate melt versus temperature. The data at 1100 and 1200 °C are after [54].

3.4. Approach to Equilibrium

To verify the approach to equilibrium, we calculated temperatures at 6 GPa using the geothermometers [61,70–72] based on the Mg-Fe^{2+} exchange between clinopyroxene and garnet. The calculations were performed using the PTEXL code developed by Thomas Koehler and Andrei Girnis (personal communication). In our calculation, we considered $Fe^{total} = Fe^{2+}$ without the effect of Fe^{3+}.

The runs in the Ecl-N2 system at 900–1000 °C exhibit a significant (by 150–300 °C) overestimation of the calculated temperatures (Table 4). This may be due either to an unsatisfactory approach to equilibrium only in experiments with the Na-rich carbonate

melt at 900–1000 °C, or the inapplicability of the thermometers to experiments with the Na-rich carbonate melt. However, in all other experiments, calculated temperatures are within 100 °C of the nominal run temperatures (Table 4). Thus, in most of the experiments, equilibrium was approached sufficiently for the question being investigated.

Table 4. Temperature estimates using Cpx-Grt geothermometers, p = 6 GPa.

System	Run	T, °C	K88	EG79	P85	K00
	D280	900	956	1116	1107	1073
	D267	950	1175	1254	1249	1233
	D253	1000	1164	1145	1131	1162
Ecl-N2	D211	1300	1404	1339	1335	1409
	D214	1400	1493	1408	1408	1498
	D217	1500	1523	1431	1433	1529
	D280	900	922	1021	1007	968
	D267	950	955	1026	1012	973
Ecl-K4	D211	1300	1384	1324	1320	1369
	D214	1400	1388	1328	1324	1370
	D217	1500	1504	1422	1425	1488

Notes: K88—[73], EG79 —[2], P85 —[74], K00—[75].

3.5. Melt—Solid Distribution Coefficients

The Fe-Mg distribution coefficients between silicate minerals and melt, $^{S/L}D(\text{Fe-Mg})$ = $^{S}(\text{Fe/Mg})/^{L}(\text{Fe/Mg})$ atomic ratio, where S—solid (Cpx, Grt, Ol) and L—liquid) are given in Table 5 and Table S5. For clinopyroxene $^{S/L}D(\text{Fe-Mg})$ is 0.41–0.68 and 0.25–0.35 in the Na- and K-bearing systems, respectively. For garnet, $^{S/L}D(\text{Fe-Mg})$ varies from 0.70 to 3.3 and for olivine $^{S/L}D(\text{Fe-Mg})$ is 0.60. The $^{S/L}D(\text{Fe-Mg})$ distribution coefficients from our experiments match the previously determined solid/melt phase equilibria under similar conditions in other experiments [42,43,54,76].

Table 5. Partition coefficients between minerals and melt.

Run no.	T,°C	$^{S/L}D(\text{Fe–Mg})$			$^{Cpx/L}D$	
		Cpx	Grt	Ol	Na$_2$O	K$_2$O
Ecl-N2						
D267	950	0.68	3.33	–	0.148	–
D253	1000	0.48	1.58	–	0.231	–
D211	1300	0.53	1.30	0.60	0.157	–
D214	1400	0.47	1.05	–	0.158	–
D217	1500	0.40	0.86	–	0.188	–
Ecl-K4						
D267	950	0.25	2.07	–	–	0.017
D211	1300	0.35	0.94	–	–	0.010
D214	1400	0.28	0.75	–	–	0.015
D217	1500	0.29	0.70	–	–	0.016

Notes: $^{Cpx/L}D(\text{Na}_2\text{O})$ = Na$_2$O^{Cpx}/Na$_2$O^{L}, $^{Cpx/L}D(\text{K}_2\text{O})$ = K$_2$O^{Cpx}/K$_2$O^{L} (weight ratio); $^{S/L}D(\text{Fe–Mg})$ = $^{S}(\text{Fe/Mg})/^{L}(\text{Fe/Mg})$, atomic ratio.

The partition coefficient of Na$_2$O (wt%) between clinopyroxene and carbonate melt, $^{Cpx/L}D(\text{Na}_2\text{O})$ = Na$_2$O^{Cpx}/Na$_2$O^{L}, established in the sodium system ranges from 0.142 to 0.237 (Table 5 and Table S5). The partition coefficient of K$_2$O (wt%), $^{Cpx/L}D(\text{K}_2\text{O})$ = K$_2$O^{Cpx}/K$_2$O^{L}, ranges from 0.01 to 0.02 (Tables 5 and S5). These values are consistent with those established in the silicate system, CaMgSi$_2$O$_6$-NaAlSi$_2$O$_6$-KAlSi$_2$O$_6$ at 6–7 GPa and 1100–1300 °C, $^{Cpx/L}D(\text{K}_2\text{O})$ = 0.02–0.11 [77] and in the carbonate-silicate system (pyroxene-K$_2$CO$_3$) at 5–14 GPa and 1400–1700 °C, $^{Cpx/L}D(\text{K}_2\text{O})$ = 0.02–0.10 [78].
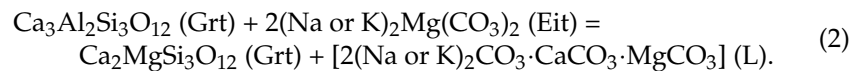
4. Discussion

4.1. Subsolidus Assemblage and Melting Reactions

The subsolidus assemblage consists of garnet, clinopyroxene, and carbonates. Although the starting carbonate mixtures are rich in $CaCO_3$, with Ca# ~70, the subsolidus assemblages in the experiments consist of eitelite in Ecl-N2 and $K_2Mg(CO_3)_2$ + magnesite in Ecl-K4 and do not contain Ca-bearing carbonates, except for the trace amount of $Na_2Ca_4(CO_3)_5$. Almost all calcium is redistributed from carbonate to garnet according to the following Ca-Mg exchange reaction:

$$3CaCO_3 \text{ (in carbonates)} + Mg_3Al2Si_3O_{12} \text{ (Grt)} =$$
$$3MgCO_3 \text{ (in carbonates)} + Ca_3Al_2Si_3O_{12} \text{ (Grt)} \tag{1}$$
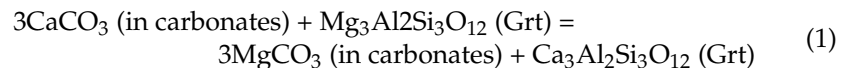
As a result of reaction (1), the garnet composition shifts from eclogite Group A to eclogite Group C (Figure 5). The pressure-induced partitioning of Ca from carbonates to garnet was reported earlier in several experimental studies on phase relations in carbonated eclogite [24,42,79].

Unlike the Ca-free subsolidus carbonates, the incipient carbonate melt has Ca# 58–60 (Figure 6b). Above the solidus, the garnet Ca# drops sharply from 49–60 to 25–30 (Figure 5, Tables 3 and S9), while eitelite and $K_2Mg(CO_3)_2$ disappear (Figure 3). Thus, at 6 GPa, the Ecl-N2 and Ecl-K4 solidi are situated at 950 °C and controlled by the following melting reaction:

$$Ca_3Al_2Si_3O_{12} \text{ (Grt)} + 2(Na \text{ or } K)_2Mg(CO_3)_2 \text{ (Eit)} =$$
$$Ca_2MgSi_3O_{12} \text{ (Grt)} + [2(Na \text{ or } K)_2CO_3 \cdot CaCO_3 \cdot MgCO_3] \text{ (L)}. \tag{2}$$
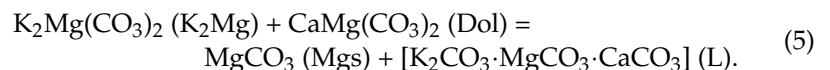
We also suppose that as pressure decreases below 6 GPa and Ca-bearing carbonates are stabilized, the Ecl-N2 and Ecl-K4 solidi will be controlled by the carbonate component. Melting of the Na- and K-carbonate (carbonatite) systems has been studied previously [45,46]. According to these data, the $Na_2Ca_4(CO_3)_5$ and then $Na_2Ca_3(CO_3)_4$ (below 4–5 GPa) compounds become stable and the solidus reactions can be approximated as follows:

$$2Na_2Mg(CO_3)_2 \text{ (Eit)} + Na_2Ca_4(CO_3)_5 \text{ (Na}_2\text{Ca}_4) =$$
$$[3Na_2CO_3 \cdot 2MgCO_3 \cdot 4CaCO_3] \text{ (L)}, \tag{3}$$

above 5 GPa and

$$2Na_2Mg(CO_3)_2 \text{ (Eit)} + Na_2Ca_3(CO_3)_5 \text{ (Na}_2\text{Ca}_3) =$$
$$[3Na_2CO_3 \cdot 2MgCO_3 \cdot 3CaCO_3] \text{ (L)}, \tag{4}$$
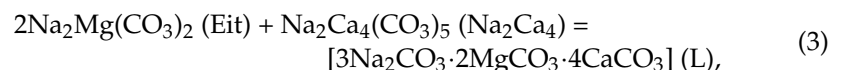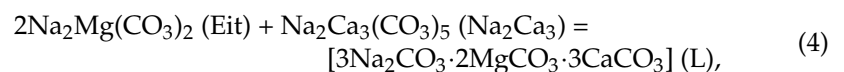
Below 4–5 GPa. In the K-carbonate system, dolomite stabilizes in addition to $K_2Mg(CO_3)_2$ yielding the following melting reaction:[-15]

$$K_2Mg(CO_3)_2 \text{ (K}_2\text{Mg)} + CaMg(CO_3)_2 \text{ (Dol)} =$$
$$MgCO_3 \text{ (Mgs)} + [K_2CO_3 \cdot MgCO_3 \cdot CaCO_3] \text{ (L)}. \tag{5}$$

According to various estimates, at 3 GPa, the alkaline carbonate or carbonatite solidus is situated at about 750–850 °C [45,46,69,80].

4.2. Comparison with the Various Solidi of the Carbonated Eclogites in Previous Experimental Studies

Phase relationships in carbonated eclogite under mantle P-T conditions have been studied in several works. The obtained solidi are shown in Figure 7. As can be seen, their temperatures differ significantly. Here we would like to discuss what this may be connected with.

Hammouda [39] studied the system OTBC consisting of 89.8 wt% basaltic glass, 10.1 wt% $CaCO_3$, and 0.12 wt% H_2O. He found that at 6 GPa and 1200 °C, the subsolidus assemblage is represented by garnet, Ca# 38, clinopyroxene, and magnesian calcite with Ca# 75. This is inconsistent with our data, according to which, at 6 GPa, garnet reacts with $CaCO_3$ to form a more calcium garnet containing up to 60 mol% grossular. As temperature increases to 1250 °C, the first melt appears, while its composition resembles subsolidus calcite and has Ca# 80. Moreover, as temperature increases above the solidus, the garnet and clinopyroxene retain their composition almost unchanged. Given that Ca-Mg-Fe carbonates with Ca# 75–80 do not melt at such low temperatures under dry conditions [62,81], it appears that, in contrast to our experiments, the solidus of the OTBC system is controlled by the melting of magnesian calcite in the presence of water.
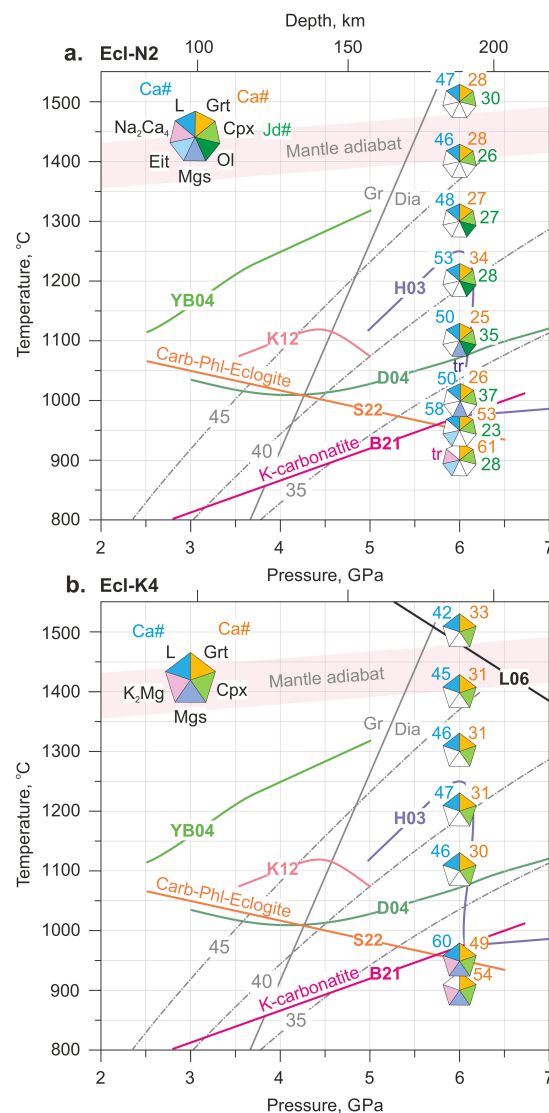
Figure 7. *P-T* plot illustrating phase relations in the Ecl-N2 (**a**) and Ecl-K4 (**b**) systems at 6 GPa in comparison with the solidi of carbonated eclogite: H03—[39], D04—[40], YB04—[42], K12—[43]; carbonated phlogopite eclogite: S22—[82]; and carbonatite: B21—[46]. The solidus of the Di-CO₂ system (L06) is after Luth [83], Gr-Dia—graphite-to-diamond phase transition [84]. The light-brown numbers, adjacent to corresponding segments in polygons, denote Ca# of garnet, Ca# of carbonate melt, and Jd# of clinopyroxene. The mantle adiabat is after [56]. The grey dash-dotted lines denote continental geotherms with a surface heat flux of 35, 40, and 45 mW/m² [85]. The data at 1100 and 1200 °C are after [54]. See the abbreviations section for mineral and phase symbols.

Dasgupta, et al. [40] reported the phase relations in the SLEC1 system, prepared by adding 5 wt% CO_2 in the form of a mixture (mole ratio): $4(Na_{0.96}K_{0.04})_2CO_3 \cdot 96(Ca_{0.32}Mg_{0.44}Fe_{0.36})$ CO_2, to an eclogite from Salt Lake crater, Oahu, Hawaii. They found that partial melting yields carbonate melt, which appears near 1080 °C at 6.1 GPa (Figure 7). Above 5 GPa, the subsolidus assemblage in the SLEC1 system is represented by garnet, clinopyroxene, magnesite, and rutile. Similar to our study, calcium carbonates are absent in the subsolidus assemblage. However, the lack of data on the composition of subsolidus carbonate phases, the composition of garnets above and below the solidus at the same pressure, and the composition of the near-solidus melt prevent inferring the melting reaction controlling the SLEC1 solidus in the range of 5.1–7.0 GPa.

Yaxley and Brey [42] studied synthetic carbonated eclogite EC1 synthesized at 3.5 GPa and 1150 °C. The mineral composition of the starting material included garnet, clinopyroxene, and calcite-dolomite solid solution. It was found that as pressure increases from 3.5 to 5.5 GPa and temperature decreases from 1275 to 1200 °C, the carbonate Ca# decreases from 86 to 56, while the garnet Ca# increases from 22 to 27. Our experiments, where garnet with Ca# 49–60 coexists with magnesite at 6 GPa and 900–950 °C, are consistent with the established pattern. However, the solidus of the EC1 system is located 400–450 °C higher than that of the Ecl-N2 and Ecl-K4 systems. The difference is due to the presence of Na and K in the subsolidus carbonates in our experiment. In contrast to our study, in the experiments by Yaxley and Brey [42], K is absent, while sodium enters clinopyroxene. As it was shown early near 6 GPa, sodium is compatible in clinopyroxene and does not enter carbonates [86]. Therefore, its fluxing effect on the solidus of carbonated eclogite is not so significant and does not exceed 50 °C [87]. Thus, melting in the EC1 system at 5.5 GPa and 1340 °C is mainly controlled by the melting of calcium dolomite, whose composition is close to the $CaCO_3$-$MgCO_3$ eutectic. This is also in good agreement with the Ca# 62 of the solidus melt, which coincides with the $CaCO_3$-$MgCO_3$ eutectic established at 1400 °C [62].

Shatskiy, et al. [43] investigated the phase relations in a K-bearing altered mid-ocean ridge basalt (MORB) + 10% $CaCO_3$. The composition of the system differs from previous works in higher contents of potassium and silica. As a result, melting in the system at 5 GPa occurs at only 1050 °C and is accompanied by the formation of a potassium aluminosilicate rather than a carbonate melt. As temperature increases to 1100 °C, the formation of two immiscible carbonate and silicate melts is observed. This behavior of the system resembles carbonated pelite (DG2) [22,88], where melting is mainly controlled by the assemblage of dolomite + K-feldspar/phengite [22,89].

Shatskiy, et al. [24] studied the phase relationships in carbonated phlogopite eclogite. They found that at 3–6 GPa, subsolidus assemblage consists of clinopyroxene, garnet, phlogopite, and Ca-Mg carbonate. As pressure increases from 3 to 6 GPa and temperature decreases from 1000 to 800 °C, the carbonate composition evolves from Mg-calcite to Ca-dolomite, dolomite, and then magnesite. At 6 GPa, melting consumes phlogopite and magnesite according to the following solidus reaction [24] accompanied by the Ca redistribution from garnet to carbonate:

$$\text{Phl } (KMg_3AlSi_3O_{10}(OH)_2) + \text{Mgs } (MgCO_3) + \text{Grs } (Ca_3Al_2Si_3O_{12}) = \qquad (6)$$
$$\text{Prp } (Mg_3Al_2Si_3O_{12}) + \text{Cpx } (CaMgSi_2O_6) + \text{L (water-bearing carbonate melt)}$$
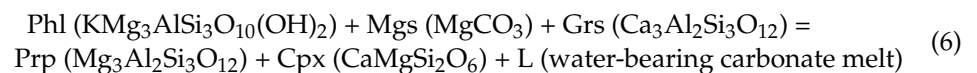
Thus, the addition of water at 6 GPa and bulk mole ratio $H_2O/K_2O \leq 2$ yields redistribution of potassium from $K_2Mg(CO_3)_2$ to phlogopite but does not affect solidus temperature at 6 GPa (Figure 7). Considering results under anhydrous conditions in K-carbonatite and Na-carbonatite systems [46], we expect a decrease in solidus temperatures of Ecl-N2 and Ecl-K4 as pressure decreases. Unlike that, the solidus of carbonated phlogopite eclogite has a negative Clapeyron slope, so that at shallower depths carbonated phlogopite eclogite becomes more refractory (Figure 7).

4.3. Composition of Carbonate Melt

In the range of 950–1200 °C, the silica content in the melt does not exceed 1.5 wt% (Figure 6). As temperature increases to 1300–1500 °C, the silica content in the melt increases

sharply to 2–6 and 7–12 wt% in the Ecl-N2 and Ecl-K4 systems, respectively. A twofold higher concentration of silica in a potassium melt correlates with a twofold higher concentration of alumina (Table S7). At 6 GPa in the aluminosilicate system, Na and K are hosted by jadeite and K-feldspar, respectively. Jadeite is poorly soluble in the carbonate melt owing to the compatibility of Na with clinopyroxene [86]. The solubility of K-feldspar in carbonate melt should be higher since K is incompatible in the aluminosilicates in presence of carbonate [22,89]. This is consistent with the lower melting temperature of the Kfs + Dol system compared to Di + Jd + 2Mgs, which is 1050 °C and 1350 °C at 6 GPa, respectively [86,89]. Although potassium doubles the solubility of SiO_2 and Al_2O_3 in the carbonate melt at 1300–1500 °C, their solubility is still low and an excess of the $KAlSi_3O_8$ component over its solubility in carbonate melt leads to the appearance of immiscible phonolitic melt [22,43,88–90].

Ca# of carbonate melt coexisting with eclogite and garnet clinopyroxenite varies from 42 to 60 (Figure 6), similar to that established in the carbonated pelite system (Ca# 52–59) [22] and in equilibrium with wehrlite (Ca# 40–60) [37,38], but higher than Ca# of K-rich carbonate melt in equilibrium with garnet lherzolite (~30–34) and harzburgite (<30) [37,38,91] (Figure 8).

Carbonate melts are very mobile owing to their excellent wetting properties, low viscosity, and density [92–96]. Therefore, carbonate melts, derived by partial melting of carbonated oceanic crust, can readily impregnate the overlying peridotitic mantle. Re-equilibration of eclogite-derived carbonate melt with peridotite should lower its Ca# and cause refertilization from harzburgite to lherzolite and wehrlitization [37].
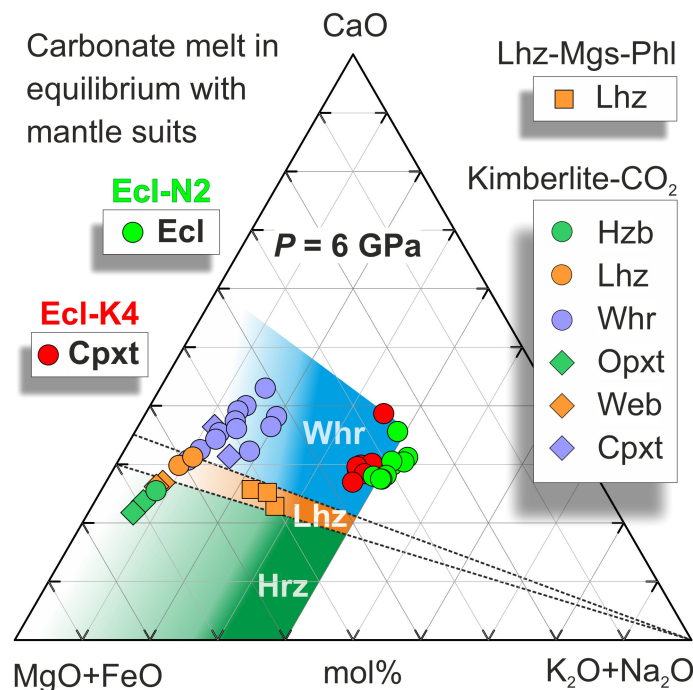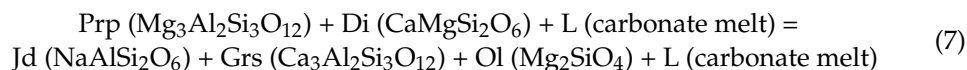

Figure 8. The pseudo-ternary projection of carbonate melt in equilibrium with bimineral eclogite in the system Ecl-N2 and clinopyroxenite in the system Ecl-K4 at 6 GPa (this study). The colored areas correspond to the compositions of the carbonate melt in equilibrium with harzburgite (green), lherzolite (brown), and wehrlite (blue) [37,38]. The compositions of the carbonate melt obtained under hydrous conditions in the system carbonated phlogopite lherzolite (Lhz-Mgs-Phl) in equilibrium with lherzolite (Lhz) are after [82]. The compositions of carbonate melt obtained in the system kimberlite-CO_2 in equilibrium with ultramafic assemblies including Hzb, Lhz, Whr, orthopyroxenite (Opxt), websterite (Web), and Cpxt are after [97].

5. Implications

5.1. Carbonatite Metasomatism

The present results show that the interaction of the Na-Ca-Mg-Fe carbonate melt with eclogite at 950–1500 °C is accompanied by an increase in the jadeite component in omphacite (Figure 4) and the grossular component in garnet (Figure 5) according to the reaction:

$$\text{Prp (Mg}_3\text{Al}_2\text{Si}_3\text{O}_{12}) + \text{Di (CaMgSi}_2\text{O}_6) + \text{L (carbonate melt)} =$$
$$\text{Jd (NaAlSi}_2\text{O}_6) + \text{Grs (Ca}_3\text{Al}_2\text{Si}_3\text{O}_{12}) + \text{Ol (Mg}_2\text{SiO}_4) + \text{L (carbonate melt)} \quad (7)$$

As a result, eclogite Group A evolves to eclogite Group B (Figures 4 and 5). In addition, reaction (4) produces olivine (Figure 3). The lack of nickel and low Mg# (86) distinguish this olivine from peridotitic olivine (Table 3 and Table S10). Similar olivine was found in a coesite-bearing diamondiferous eclogite xenolith along with secondary metasomatic mineralization including phlogopite, K-feldspar, orthopyroxene, and secondary clinopyroxene [98,99].

The interaction of the K-Ca-Mg-Fe carbonate melt with the eclogite lowers the sodium in the clinopyroxene and shifts the composition of the eclogite towards garnet clinopyroxenite (Figure 4). The above tendency may explain the formation of Na- and Al-depleted clinopyroxene with 'spongy' texture replacing primary omphacite in diamondiferous eclogites [1,100,101]. High potassium concentrations, up to 0.6 wt% K_2O, in this clinopyroxene [1] indicate its deep, >3 GPa, origin [102]. Moreover, this indicates that the metasomatic melt was rich in potassium [78,103]. A direct finding of the K- and Cl-rich carbonatite melt as microinclusions in diamonds in the alteration veins in the eclogite xenoliths containing Na-poor 'spongy' textured clinopyroxene [8] supports our experimental observations.

5.2. Hosts for Potassium in Carbonated Eclogite

Present experiments on the K-rich carbonated eclogite system suggest that under water-poor conditions at 6 GPa, potassium enters $K_2Mg(CO_3)_2$. This is supported by the findings of $K_2Mg(CO_3)_2$ microinclusions in kimberlitic diamonds [20]. In contrast, under hydrous conditions, potassium is mainly hosted by phlogopite, as shown experimentally in the systems KMAS–H_2O–CO_2 [104], KCMAS–H_2O–CO_2 [105], and carbonated phlogopite eclogite [82]. This is also confirmed by the findings of syngenetic phlogopite inclusions in lithospheric diamonds [55,106–108] and diamondiferous eclogite xenoliths [1,2]. Thus, in the presence of volatiles (CO_2 and/or H_2O), potassium is hosted either by $K_2Mg(CO_3)_2$ containing 40 wt% K_2O, or phlogopite containing 11 wt% K_2O, or carbonate melt containing up to 30 wt% K_2O.

5.3. The Link between Kimberlites and Mantle Carbonatites

Although the temperatures in our experiments cover the entire range of geotherms of the lithospheric and the asthenospheric mantle at a depth of 200 km [56,85], no gradual transition from carbonate to kimberlite-like carbonate-silicate melt was observed. The highest silica content (7–12 wt% SiO_2) in the obtained melt is comparable with that in the alkali-poor (9–15 wt% SiO_2) and K-rich (12–16 wt% SiO_2) carbonate melts in equilibrium with natural peridotite at 6 GPa and 1500 °C [37,91,109]. This is consistent with the idea that during ascent through the lithospheric mantle, the kimberlite magma was a combination of alkaline carbonate melt and solid silicate matter (xenoliths and xenocrysts) [25,28,29]. Decarbonation [110] and the subsequent loss of CO_2 during the explosive emplacement of the kimberlites [111] led to a significant loss of the carbonate component and solidification of kimberlite magma in the form of silicate rock. Postmagmatic leaching of the alkaline carbonates that withstood decarbonation reinforces this trend [28,29]. The essentially carbonate composition of the liquid component of kimberlite magma is confirmed by the alkaline carbonate composition of inclusions in kimberlite magmatic minerals and xenoliths [24,25,27,33–35], as well as experiments on kimberlite melting [97,112,113].

Sokol et al. [114] have experimentally shown that a successive increase in the water content from 2.5 to 11.6 wt% in the kimberlite magma system over 6.3–7.5 GPa and 1400–1500 °C promotes the fusion of the silicate constituent yielding the transformation of the melt from essentially carbonate (5–12 wt% SiO_2 at 2.5 wt% H_2O) to carbonate-silicate (17–19 wt% SiO_2 at 6–6.5 wt% H_2O) and finally complete melting of kimberlite at 11–12 wt% H_2O. Comparing these data with the alkaline carbonatitic composition of the melt inclusions in the igneous minerals of the kimberlites worldwide [24,25,27], we conclude that the water content in kimberlite magma did not exceed a few percent.

Supplementary Materials: The following supporting information can be downloaded at: https://www.mdpi.com/article/10.3390/min13010082/s1, Table S1: Composition of natural eclogite used as a component of starting mixtures; Table S2: Compositions of carbonate component of starting mixtures; Table S3: Compositions of starting mixtures made of carbonates and natural eclogite; Table S4: Summary of run conditions, composition of phases (in mol% and wt%) and mole/weight fraction of phases (MFP/WFP) from experiments on the interaction of eclogite with carbonatitic melts at 6.0 GPa and 900–1500 °C; Table S5: Calculation of mole fraction of phases (MFP) from experiments on the interaction eclogite with carbonatitic melts at 6.0 GPa and 900–1500 °C; Table S6: Calculation of weight fraction of phases (WFP) from experiments on the interaction eclogite with carbonatitic melts at 6.0 GPa and 900–1500 °C; Table S7: Compositions of carbonatitic melts (L) from experiments on the interaction of eclogite with carbonatitic melts at 6.0 GPa and 900–1500 °C; Table S8: Compositions of clinopyroxenes (Cpx) from experiments on the interaction of eclogite with carbonatitic melts at 6.0 GPa and 900–1500 °C; Table S9: Compositions of garnets (Grt) from experiments on the interaction of eclogite with carbonatitic melts at 6.0 GPa and 900–1500 °C; Table S10: Compositions of olivine (Grt) from experiments on the interaction of eclogite with carbonatitic melts at 6.0 GPa and 900–1500 °C; Table S7: Compositions of carbonate from experiments on the interaction of eclogite with carbonatitic melts at 6.0 GPa and 900–1500 °C; Table S8: Compositions of clinopyroxenes (Cpx) from experiments on the interaction of eclogite with carbonatitic melts at 6.0 GPa and 900–1500 °C; Table S9: Compositions of garnets (Grt) from experiments on the interaction of eclogite with carbonatitic melts at 6.0 GPa and 900–1500 °C; Table S10: Compositions of olivine (Grt) from experiments on the interaction of eclogite with carbonatitic melts at 6.0 GPa and 900–1500 °C; Table S11: Compositions of carbonate from experiments on the interaction of eclogite with carbonatitic melts at 6.0 GPa and 900–1500 °C.

Author Contributions: Conceptualization, A.S.; methodology, A.S. and K.D.L.; validation, K.D.L.; formal analysis, A.B., A.V.A., and A.S.; investigation, A.B.; resources, K.D.L.; data curation, A.B. and A.S.; writing—original draft preparation, A.B. and A.S.; writing—review and editing, A.S.; visualization, A.B. and A.S.; supervision, A.S.; project administration, A.S. and A.B.; funding acquisition, A.V.A. All authors have read and agreed to the published version of the manuscript.

Institutional Review Board Statement: Not applicable.

Informed Consent Statement: Not applicable.

Data Availability Statement: Not applicable.

Conflicts of Interest: The authors declare no conflict of interest.

Abbreviations

Alm—almandine, Arg — aragonite, Cal—calcite, Cpx—clinopyroxene, Cpxt—clinopyroxenite, Di—diopside, Dol—dolomite, Ecl—eclogite, Eit—eitelite $Na_2Mg(CO_3)_2$, Gr—graphite, Grs —grossular, Grt—garnet, Hd—hedendergite, Hrz—harzburgite, Jd—jadeite, K_2Mg–$K_2Mg(CO_3)_2$, L—carbonate melt, Lhz—lherzolite, Mgs—magnesite, Na_2Ca_4 –$Na_2Ca_4(CO_3)_5$, Ol—olivine, Opxt—orthopyroxenite, Prp—

pyrope, q-Cpx—quench clinopyroxene, Ca# = 100·Ca/(Ca + Mg), Web—websterite, Whr—wehrlite.

References

1. Shatsky, V.; Ragozin, A.; Zedgenizov, D.; Mityukhin, S. Evidence for multistage evolution in a xenolith of diamond-bearing eclogite from the Udachnaya kimberlite pipe. *Lithos* **2008**, *105*, 289–300. [CrossRef]
2. Smart, K.A.; Heaman, L.M.; Chacko, T.; Simonetti, A.; Kopylova, M.; Mah, D.; Daniels, D. The origin of high-MgO diamond eclogites from the Jericho Kimberlite, Canada. *Earth Planet. Sci. Lett.* **2009**, *284*, 527–537. [CrossRef]
3. Agashev, A.M.; Pokhilenko, L.N.; Pokhilenko, N.P.; Shchukina, E.V. Geochemistry of eclogite xenoliths from the Udachnaya Kimberlite Pipe: Section of ancient oceanic crust sampled. *Lithos* **2018**, *314–315*, 187–200. [CrossRef]
4. Aulbach, S.; Viljoen, K.S.; Gerdes, A. Diamondiferous and barren eclogites and pyroxenites from the western Kaapvaal craton record subduction processes and mantle metasomatism, respectively. *Lithos* **2020**, *368*, 105588. [CrossRef]
5. Taylor, L.A.; Keller, R.A.; Snyder, G.A.; Wang, W.; Carlson, W.D.; Hauri, E.H.; Mccandless, T.; Kim, K.-R.; Sobolev, N.V.; Bezborodov, S.M. Diamonds and their mineral inclusions, and what they tell us: A detailed "pull-apart" of a diamondiferous eclogite. *Int. Geol. Rev.* **2000**, *42*, 959–983. [CrossRef]
6. Anand, M.; Taylor, L.A.; Misra, K.C.; Carlson, W.D.; Sobolev, N.V. Nature of diamonds in Yakutian eclogites: Views from eclogite tomography and mineral inclusions in diamonds. *Lithos* **2004**, *77*, 333–348. [CrossRef]
7. Taylor, L.A.; Anand, M. Diamonds: Time capsules from the Siberian Mantle. *Geochemistry* **2004**, *64*, 1–74. [CrossRef]
8. Zedgenizov, D.A.; Ragozin, A.L.; Shatsky, V.S.; Griffin, W.L. Diamond formation during metasomatism of mantle eclogite by chloride-carbonate melt. *Contrib. Mineral. Petrol.* **2018**, *173*, 84. [CrossRef]
9. Zedgenizov, D.; Ragozin, A.; Shatsky, V. Chloride-carbonate fluid in diamonds from the eclogite xenolith. In *Doklady Earth Sciences*; Springer Nature BV: Berlin/Heidelberg, Germany, 2007; pp. 961–964.
10. Schrauder, M.; Navon, O. Hydrous and carbonatitic mantle fluids in fibrous diamonds from Jwaneng, Botswana. *Geochim. Et Cosmochim. Acta* **1994**, *58*, 761–771. [CrossRef]
11. Klein-BenDavid, O.; Izraeli, E.S.; Hauri, E.; Navon, O. Mantle fluid evolution—A tale of one diamond. *Lithos* **2004**, *77*, 243–253. [CrossRef]
12. Klein-BenDavid, O.; Izraeli, E.S.; Hauri, E.; Navon, O. Fluid inclusions in diamonds from the Diavik mine, Canada and the evolution of diamond-forming fluids. *Geochim. Et Cosmochim. Acta* **2007**, *71*, 723–744. [CrossRef]
13. Zedgenizov, D.A.; Rege, S.; Griffin, W.L.; Kagi, H.; Shatsky, V.S. Composition of trapped fluids in cuboid fibrous diamonds from the Udachnaya kimberlite: LAM-ICPMS analysis. *Chem. Geol.* **2007**, *240*, 151–162. [CrossRef]
14. Klein-BenDavid, O.; Logvinova, A.M.; Schrauder, M.; Spetius, Z.V.; Weiss, Y.; Hauri, E.H.; Kaminsky, F.V.; Sobolev, N.V.; Navon, O. High-Mg carbonatitic microinclusions in some Yakutian diamonds—A new type of diamond-forming fluid. *Lithos* **2009**, *112*, 648–659. [CrossRef]
15. Weiss, Y.; Kessel, R.; Griffin, W.L.; Kiflawi, I.; Klein-BenDavid, O.; Bell, D.R.; Harris, J.W.; Navon, O. A new model for the evolution of diamond-forming fluids: Evidence from microinclusion-bearing diamonds from Kankan, Guinea. *Lithos* **2009**, *112*, 660–674. [CrossRef]
16. Zedgenizov, D.A.; Ragozin, A.L.; Shatsky, V.S.; Araujo, D.; Griffin, W.L.; Kagi, H. Mg and Fe-rich carbonate-silicate high-density fluids in cuboid diamonds from the Internationalnaya kimberlite pipe (Yakutia). *Lithos* **2009**, *112*, 638–647. [CrossRef]
17. Skuzovatov, S.Y.; Zedgenizov, D.A.; Shatsky, V.S.; Ragozin, A.L.; Kuper, K.E. Composition of cloudy microinclusions in octahedral diamonds from the Internatsional'naya kimberlite pipe (Yakutia). *Russ. Geol. Geophys.* **2011**, *52*, 85–96. [CrossRef]
18. Zedgenizov, D.A.; Ragozin, A.L.; Shatsky, V.S.; Araujo, D.; Griffin, W.L. Fibrous diamonds from the placers of the northeastern Siberian Platform: Carbonate and silicate crystallization media. *Russ. Geol. Geophys.* **2011**, *52*, 1298–1309. [CrossRef]
19. Weiss, Y.; Kiflawi, I.; Davies, N.; Navon, O. High-density fluids and the growth of monocrystalline diamonds. *Geochim. Et Cosmochim. Acta* **2014**, *141*, 145–159. [CrossRef]
20. Jablon, B.M.; Navon, O. Most diamonds were created equal. *Earth Planet. Sci. Lett.* **2016**, *443*, 41–47. [CrossRef]
21. Skuzovatov, S.; Zedgenizov, D.; Howell, D.; Griffin, W.L. Various growth environments of cloudy diamonds from the Malobotuobia kimberlite field (Siberian craton). *Lithos* **2016**, *265*, 96–107. [CrossRef]
22. Shatskiy, A.; Arefiev, A.V.; Podborodnikov, I.V.; Litasov, K.D. Origin of K-rich diamond-forming immiscible melts and CO$_2$ fluid via partial melting of carbonated pelites at a depth of 180–200 km. *Gondwana Res.* **2019**, *75*, 154–171. [CrossRef]
23. Gubanov, N.; Zedgenizov, D.; Sharygin, I.; Ragozin, A. Origin and evolution of high-Mg carbonatitic and low-Mg carbonatitic to silicic high-density fluids in coated diamonds from Udachnaya kimberlite pipe. *Minerals* **2019**, *9*, 734. [CrossRef]
24. Golovin, A.V.; Sharygin, I.S.; Korsakov, A.V. Origin of alkaline carbonates in kimberlites of the Siberian craton: Evidence from melt inclusions in mantle olivine of the Udachnaya-East pipe. *Chem. Geol.* **2017**, *455*, 357–375. [CrossRef]
25. Kamenetsky, V.S.; Kamenetsky, M.B.; Weiss, Y.; Navon, O.; Nielsen, T.F.D.; Mernagh, T.P. How unique is the Udachnaya-East kimberlite? Comparison with kimberlites from the Slave Craton (Canada) and SW Greenland. *Lithos* **2009**, *112*, 334–346. [CrossRef]
26. Abersteiner, A.; Kamenetsky, V.S.; Goemann, K.; Giuliani, A.; Howarth, G.H.; Castillo-Oliver, M.; Thompson, J.; Kamenetsky, M.; Cherry, A. Composition and emplacement of the Benfontein kimberlite sill complex (Kimberley, South Africa): Textural, petrographic and melt inclusion constraints. *Lithos* **2019**, *324*, 297–314. [CrossRef]

27.   Abersteiner, A.; Giuliani, A.; Kamenetsky, V.S.; Phillips, D. Petrographic and melt-inclusion constraints on the petrogenesis of a magmaclast from the Venetia kimberlite cluster, South Africa. *Chem. Geol.* **2017**, *455*, 331–341. [CrossRef]

28.   Kamenetsky, V.S.; Golovin, A.V.; Maas, R.; Giuliani, A.; Kamenetsky, M.B.; Weiss, Y. Towards a new model for kimberlite petrogenesis: Evidence from unaltered kimberlites and mantle minerals. *Earth-Sci. Rev.* **2014**, *139*, 145–167. [CrossRef]

29.   Kamenetsky, M.B.; Sobolev, A.V.; Kamenetsky, V.S.; Maas, R.; Danyushevsky, L.V.; Thomas, R.; Pokhilenko, N.P.; Sobolev, N.V. Kimberlite melts rich in alkali chlorides and carbonates: A potent metasomatic agent in the mantle. *Geology* **2004**, *32*, 845–848. [CrossRef]

30.   Giuliani, A.; Kamenetsky, V.S.; Phillips, D.; Kendrick, M.A.; Wyatt, B.A.; Goemann, K. Nature of alkali-carbonate fluids in the sub-continental lithospheric mantle. *Geology* **2012**, *40*, 967–970. [CrossRef]

31.   Sharygin, I.S.; Golovin, A.V.; Korsakov, A.V.; Pokhilenko, N.P. Eitelite in sheared peridotite xenoliths from Udachnaya-East kimberlite pipe (Russia)—A new locality and host rock type. *Eur. J. Mineral.* **2013**, *25*, 825–834. [CrossRef]

32.   Golovin, A.; Sharygin, I.; Kamenetsky, V.; Korsakov, A.; Yaxley, G. Alkali-carbonate melts from the base of cratonic lithospheric mantle: Links to kimberlites. *Chem. Geol.* **2018**, *483*, 261–274. [CrossRef]

33.   Golovin, A.V.; Sharygin, I.S.; Korsakov, A.V.; Kamenetsky, V.S.; Abersteiner, A. Can primitive kimberlite melts be alkali-carbonate liquids: Composition of the melt snapshots preserved in deepest mantle xenoliths. *J. Raman Spectrosc.* **2020**, *51*, 1849–1867. [CrossRef]

34.   Sharygin, I.S.; Golovin, A.V.; Dymshits, A.M.; Kalugina, A.D.; Solovev, K.A.; Malkovets, V.G.; Pokhilenko, N.P. Relics of deep alkali–carbonate melt in the mantle xenolith from the Komsomolskaya–Magnitnaya kimberlite pipe (Upper Muna field, Yakutia). *Dokl. Earth Sci.* **2021**, *500*, 842–847. [CrossRef]

35.   Sharygin, I.S.; Golovin, A.V.; Tarasov, A.A.; Dymshits, A.M.; Kovaleva, E. Confocal Raman spectroscopic study of melt inclusions in olivine of mantle xenoliths from the Bultfontein kimberlite pipe (Kimberley cluster, South Africa): Evidence for alkali-rich carbonate melt in the mantle beneath Kaapvaal Craton. *J. Raman Spectrosc.* **2022**, *53*, 508–524. [CrossRef]

36.   Shatskiy, A.; Litasov, K.D.; Borzdov, Y.M.; Katsura, T.; Yamazaki, D.; Ohtani, E. Silicate diffusion in alkali-carbonatite and hydrous melts at 16.5 and 24 GPa: Implication for the melt transport by dissolution-precipitation in the transition zone and uppermost lower mantle. *Phys. Earth Planet. Inter.* **2013**, *225*, 1–11. [CrossRef]

37.   Amundsen, H.E.F. Evidence for liquid immiscibility in the upper mantle. *Nature* **1987**, *327*, 692–695. [CrossRef]

38.   Sumiya, H.; Yusa, H.; Inoue, T.; Ofuji, H.; Irifune, T. Conditions and mechanism of formation of nano-polycrystalline diamonds on direct transformation from graphite and non-graphitic carbon at high pressure and temperature. *High Press. Res.* **2006**, *26*, 63–69. [CrossRef]

39.   Hammouda, T. High-pressure melting of carbonated eclogite and experimental constraints on carbon recycling and storage in the mantle. *Earth Planet. Sci. Lett.* **2003**, *214*, 357–368. [CrossRef]

40.   Dasgupta, R.; Hirschmann, M.M.; Withers, A.C. Deep global cycling of carbon constrained by the solidus of anhydrous, carbonated eclogite under upper mantle conditions. *Earth Planet. Sci. Lett.* **2004**, *227*, 73–85. [CrossRef]

41.   Dasgupta, R.; Hirschmann, M.M.; Dellas, N. The effect of bulk composition on the solidus of carbonated eclogite from partial melting experiments at 3 GPa. *Contrib. Mineral. Petrol.* **2005**, *149*, 288–305. [CrossRef]

42.   Yaxley, G.M.; Brey, G.P. Phase relations of carbonate-bearing eclogite assemblages from 2.5 to 5.5 GPa: Implications for petrogenesis of carbonatites. *Contrib. Mineral. Petrol.* **2004**, *146*, 606–619. [CrossRef]

43.   Kiseeva, E.S.; Yaxley, G.M.; Hermann, J.; Litasov, K.D.; Rosenthal, A.; Kamenetsky, V.S. An experimental study of carbonated eclogite at 3.5–5.5 GPa—Implications for silicate and carbonate metasomatism in the cratonic mantle. *J. Petrol.* **2012**, *53*, 727–759. [CrossRef]

44.   Shirasaka, M.; Takahashi, E. A genesis of carbonatitic melt within subducting oceanic crust: High pressure experiments in the system MORB-CaCO₃. In Proceedings of the 8th International Kimberlite Conference Long Abstract, Victoria, BC, Canada, 22–27 June 2003; pp. 1–5.

45.   Litasov, K.D.; Shatskiy, A.; Ohtani, E.; Yaxley, G.M. The solidus of alkaline carbonatite in the deep mantle. *Geology* **2013**, *41*, 79–82. [CrossRef]

46.   Bekhtenova, A.; Shatskiy, A.; Podborodnikov, I.V.; Arefiev, A.V.; Litasov, K.D. Phase relations in carbonate component of carbonatized eclogite and peridotite along subduction and continental geotherms. *Gondwana Res.* **2021**, *94*, 186–200. [CrossRef]

47.   Bustarret, E.; Gheeraert, E.; Watanabe, K. Optical and electronic properties of heavily boron-doped homo-epitaxial diamond. *Phys. Status Solidi* **2003**, *199*, 9–18. [CrossRef]

48.   Shatskiy, A.; Litasov, K.D.; Sharygin, I.S.; Egonin, I.A.; Mironov, A.M.; Palyanov, Y.N.; Ohtani, E. The system Na₂CO₃–CaCO₃– MgCO₃ at 6 GPa and 900–1250 °C and its relation to the partial melting of carbonated mantle. *High Press. Res.* **2016**, *36*, 23–41. [CrossRef]

49.   Pyle, J.M.; Haggerty, S.E. Silicate-carbonate liquid immiscibility in upper-mantle eclogites: Implications for natrosilicic and carbonatitic conjugate melts. *Geochim. Et Cosmochim. Acta* **1994**, *58*, 2997–3011. [CrossRef]

50.   Girnis, A.; Bulatov, V.; Brey, G.; Gerdes, A.; Höfer, H. Trace element partitioning between mantle minerals and silico-carbonate melts at 6–12GPa and applications to mantle metasomatism and kimberlite genesis. *Lithos* **2013**, *160*, 183–200. [CrossRef]

51.   Pal'yanov, Y.N.; Sokol, A.G.; Borzdov, Y.M.; Khokhryakov, A.F.; Sobolev, N.V. Diamond formation from mantle carbonate fluids. *Nature* **1999**, *400*, 417–418. [CrossRef]

52. Navon, O.; Hutcheon, I.; Rossman, G.; Wasserburg, G. Mantle-derived fluids in diamond micro-inclusions. *Nature* **1988**, *335*, 784–789. [CrossRef]

53. Weiss, Y.; Czas, J.; Navon, O. Fluid inclusions in fibrous diamonds. *Rev. Mineral. Geochem.* **2022**, *88*, 475–532. [CrossRef]

54. Shatskiy, A.; Bekhtenova, A.; Podborodnikov, I.V.; Arefiev, A.V.; Litasov, K.D. Carbonate melt interaction with natural eclogite at 6 GPa and 1100–1200 °C: Implications for metasomatic melt composition in subcontinental lithospheric mantle. *Chem. Geol.* **2020**, *558*, 119915. [CrossRef]

55. Shirey, S.B.; Cartigny, P.; Frost, D.J.; Keshav, S.; Nestola, F.; Nimis, P.; Pearson, D.G.; Sobolev, N.V.; Walter, M.J. Diamonds and the geology of mantle carbon. *Rev. Mineral. Geochem.* **2013**, *75*, 355–421. [CrossRef]

56. Katsura, T. A revised adiabatic temperature profile for the mantle. *J. Geophys.Res. Solid Earth* **2022**, *127*, e2021JB023562. [CrossRef]

57. Ragozin, A.L.; Palyanov, Y.N.; Zedgenizov, D.A.; Kalinin, A.A.; Shatsky, V.S. The homogenization of carbonate-containing microinclusions in diamond at P-T parameters of the upper mantle. *Doklady Akademii Nauk* in press. **2016**.

58. Ragozin, A.L.; Karimova, A.A.; Litasov, K.D.; Zedgenizov, D.A.; Shatsky, V.S. The water content in mantle xenoliths from Udachnaya pipe (Yakutia). *Russ. Geol. Geophys.* **2014**, *55*, 428–442. [CrossRef]

59. Taylor, L.A.; Neal, C.R. Eclogites with oceanic crustal and mantle signatures from the Bellsbank kimberlite, South Africa, Part I: Mineralogy, petrography, and whole rock chemistry. *J. Geol.* **1989**, *97*, 551–567. [CrossRef]

60. Coleman, R.G.; Lee, D.E.; Beatty, L.B.; Brannock, W.W. Eclogites and eclogites: Their differences and similarities. *Geol. Soc. Am. Bull.* **1965**, *76*, 483–508. [CrossRef]

61. Ellis, D.J.; Green, D.H. An experimental study of the effect of Ca upon garnet-clinopyroxene Fe-Mg exchange equilibria. *Contrib. Mineral. Petrol.* **1979**, *71*, 13–22. [CrossRef]

62. Sidorov, V.; Ekimov, E.; Stishov, S.; Bauer, E.; Thompson, J. Superconducting and normal-state properties of heavily hole-doped diamond. *Phys. Rev. B* **2005**, *71*, 060502. [CrossRef]

63. Shatskiy, A.; Litasov, K.D.; Terasaki, H.; Katsura, T.; Ohtani, E. Performance of semi-sintered ceramics as pressure-transmitting media up to 30 GPa. *High Press. Res.* **2010**, *30*, 443–450. [CrossRef]

64. Hernlund, J.; Leinenweber, K.; Locke, D.; Tyburczy, J.A. A numerical model for steady-state temperature distributions in solid-medium high-pressure cell assemblies. *Am. Mineral.* **2006**, *91*, 295–305. [CrossRef]

65. Shatskiy, A.; Sharygin, I.S.; Gavryushkin, P.N.; Litasov, K.D.; Borzdov, Y.M.; Shcherbakova, A.V.; Higo, Y.; Funakoshi, K.-I.; Palyanov, Y.N.; Ohtani, E. The system K_2CO_3-$MgCO_3$ at 6 GPa and 900–1450 °C. *Am. Mineral.* **2013**, *98*, 1593–1603. [CrossRef]

66. Brey, G.P.; Kohler, T. Geothermobarometry in four-phase lherzolites II. New thermobarometers, and practical assessment of existing thermobarometers. *J. Petrol.* **1990**, *31*, 1353–1378. [CrossRef]

67. Lavrent'ev, Y.G.; Karmanov, N.S.; Usova, L.V. Electron probe microanalysis of minerals: Microanalyzer or scanning electron microscope? *Russ. Geol. Geophys.* **2015**, *56*, 1154–1161. [CrossRef]

68. Newbury, D.E.; Ritchie, N.W.M. Performing elemental microanalysis with high accuracy and high precision by scanning electron microscopy/silicon drift detector energy-dispersive X-ray spectrometry (SEM/SDD-EDS). *J. Mater. Sci.* **2015**, *50*, 493–518. [CrossRef]

69. Arefiev, A.V.; Shatskiy, A.; Podborodnikov, I.V.; Behtenova, A.; Litasov, K.D. The system K_2CO_3–$CaCO_3$–$MgCO_3$ at 3 GPa: Implications for carbonatite melt compositions in the subcontinental lithospheric mantle. *Minerals* **2019**, *9*, 296. [CrossRef]

70. Powell, R. Regression diagnostics and robust regression in geothermometer/geobarometer calibration: The garnet-clinopyroxene geothermometer revisited. *J. Metamorph. Geol.* **1985**, *3*, 231–243. [CrossRef]

71. Krogh Ravna, E. The garnet–clinopyroxene Fe^{2+}–Mg geothermometer: An updated calibration. *J. Metamorph. Geol.* **2000**, *18*, 211–219. [CrossRef]

72. Krogh, E.J. The garnet-clinopyroxene Fe-Mg geothermometer—A reinterpretation of existing experimental data. *Contrib. Mineral. Petrol.* **1988**, *99*, 44–48. [CrossRef]

73. Korsakov, A.V.; Dieing, T.; Golovin, A.V.; Toporski, J. Raman imaging of fluid inclusions in garnet from UHPM rocks (Kokchetav massif, Northern Kazakhstan). *Spectrochim. Acta Part A Mol. Biomol. Spectrosc.* **2011**, *80*, 88–95. [CrossRef]

74. Dawson, J.B. Contrasting types of upper-mantle metasomatism. In *Developments in Petrology*; Elsevier: Amsterdam, The Netherlands, 1984; Volume 11, pp. 289–294.

75. McNeil, A.M.; Edgar, A.D. Sodium-rich metasomatism in the upper mantle: Implications of experiments on the pyrolite-Na_2O-rich fluid system at 950 °C, 20 kbar. *Geochim. Et Cosmochim. Acta* **1987**, *51*, 2285–2294. [CrossRef]

76. Dasgupta, R.; Hirschmann, M.M. A modified iterative sandwich method for determination of near-solidus partial melt compositions. II. Application to determination of near-solidus melt compositions of carbonated peridotite. *Contrib. Mineral. Petrol.* **2007**, *154*, 647–661. [CrossRef]

77. Safonov, O.G.; Litvin, Y.A.; Perchuk, L.L. Synthesis of omphacites and isomorphic features of clinopyroxenes in the system $CaMgSi_2O_6$-$NaAlSi_2O_6$-$KAlSi_2O_6$. *Petrology* **2004**, *12*, 70–81.

78. Harlow, G.E. K in clinopyroxene at high pressure and temperature: An experimental study. *Am. Mineral.* **1997**, *82*, 259–269. [CrossRef]

79. Yaxley, G.M.; Green, D.H. Experimental demonstration of refractory carbonate-bearing eclogite and siliceous melt in the subduction regime. *Earth Planet. Sci. Lett.* **1994**, *128*, 313–325. [CrossRef]

80. Safonov, O.G.; Perchuk, L.L.; Yapaskurt, V.O.; Litvin, Y.A. Immiscibility of carbonate-silicate and chloride-carbonate melts in the kimberlite-$CaCO_3$–Na_2CO_3–KCl system at 4.8 GPa. *Dokl. Earth Sci.* **2009**, *424*, 388–392. [CrossRef]

81. Shatskiy, A.; Borzdov, Y.M.; Litasov, K.D.; Kupriyanov, I.N.; Ohtani, E.; Palyanov, Y.N. Phase relations in the system $FeCO_3$-$CaCO_3$ at 6 GPa and 900–1700 °C and its relation to the system $CaCO_3$-$FeCO_3$-$MgCO_3$. *Am. Mineral.* **2014**, *99*, 773–785. [CrossRef]

82. Harker, R.I.; Tuttle, O.F. Studies in the system CaO-MgO-CO_2; Part 1, The thermal dissociation of calcite, dolomite and magnesite. *Am. J. Sci.* **1955**, *253*, 209–224. [CrossRef]

83. Luth, R.W. Experimental study of the $CaMgSi_2O_6$-CO_2 system at 3–8 GPa. *Contrib. Mineral. Petrol.* **2006**, *151*, 141–157. [CrossRef]

84. Day, H.W. A revised diamond-graphite transition curve. *Am. Mineral.* **2012**, *97*, 52–62. [CrossRef]

85. Hasterok, D.; Chapman, D.S. Heat production and geotherms for the continental lithosphere. *Earth Planet. Sci. Lett.* **2011**, *307*, 59–70. [CrossRef]

86. Irifune, T.; Isobe, F.; Shinmei, T. A novel large-volume Kawai-type apparatus and its application to the synthesis of sintered bodies of nano-polycrystalline diamond. *Phys. Earth Planet. Inter.* **2014**, *228*, 255–261. [CrossRef]

87. Shatskiy, A.; Podborodnikov, I.V.; Arefiev, A.V.; Bekhtenova, A.; Vinogradova, Y.G.; Stepanov, K.M.; Litasov, K.D. Pyroxene-carbonate reactions in the $CaMgSi_2O_6 \pm NaAlSi_2O_6 + MgCO_3 \pm Na_2CO_3 \pm K_2CO_3$ system at 3–6 GPa: Implications for partial melting of carbonated peridotite. *Contrib. Mineral. Petrol.* **2021**, *176*, 34. [CrossRef]

88. Thomsen, T.B.; Schmidt, M.W. Melting of carbonated pelites at 2.5–5.0 GPa, silicate–carbonatite liquid immiscibility, and potassium–carbon metasomatism of the mantle. *Earth Planet. Sci. Lett.* **2008**, *267*, 17–31. [CrossRef]

89. Shatskiy, A.; Arefiev, A.V.; Podborodnikov, I.V.; Litasov, K.D. Liquid immiscibility and phase relations in the join $KAlSi_3O_8$–$CaMg(CO_3)_2 \pm NaAlSi_2O_6 \pm Na_2CO_3$ at 6 GPa: Implications for diamond-forming melts. *Chem. Geol.* **2020**, *550*, 119701. [CrossRef]

90. Shatskiy, A.; Arefiev, A.V.; Podborodnikov, I.V.; Litasov, K.D. Effect of water on carbonate-silicate liquid immiscibility in the system $KAlSi_3O_8$–$CaMgSi_2O_6$–$NaAlSi_2O_6$–$CaMg(CO_3)_2$ at 6 GPa: Implications for diamond-forming melts. *Am. Mineral.* **2021**, *106*, 165–173. [CrossRef]

91. Brey, G.P.; Bulatov, V.K.; Girnis, A.V. Melting of K-rich carbonated peridotite at 6–10 GPa and the stability of K-phases in the upper mantle. *Chem. Geol.* **2011**, *281*, 333–342. [CrossRef]

92. Minarik, W.G.; Watson, E.B. Interconnectivity of carbonate melt at low melt fraction. *Earth Planet. Sci. Lett.* **1995**, *133*, 423–437. [CrossRef]

93. Dobson, D.P.; Jones, A.P.; Rabe, R.; Sekine, T.; Kurita, K.; Taniguchi, T.; Kondo, T.; Kato, T.; Shimomura, O.; Urakawa, S. In-situ measurement of viscosity and density of carbonate melts at high pressure. *Earth Planet. Sci. Lett.* **1996**, *143*, 207–215. [CrossRef]

94. Hammouda, T.; Laporte, D. Ultrafast mantle impregnation by carbonatite melts. *Geology* **2000**, *28*, 283–285. [CrossRef]

95. Kono, Y.; Kenney-Benson, C.; Hummer, D.; Ohfuji, H.; Park, C.; Shen, G.; Wang, Y.; Kavner, A.; Manning, C.E. Ultralow viscosity of carbonate melts at high pressures. *Nat. Commun.* **2014**, *5*, 5091. [CrossRef]

96. Stagno, V.; Stopponi, V.; Kono, Y.; Manning, C.E.; Irifune, T. Experimental determination of the viscosity of Na_2CO_3 melt between 1.7 and 4.6 GPa at 1200–1700°C: Implications for the rheology of carbonatite magmas in the Earth's upper mantle. *Chem. Geol.* **2018**, *501*, 19–25. [CrossRef]

97. Shatskiy, A.; Litasov, K.D.; Sharygin, I.S.; Ohtani, E. Composition of primary kimberlite melt in a garnet lherzolite mantle source: Constraints from melting phase relations in anhydrous Udachnaya-East kimberlite with variable CO_2 content at 6.5 GPa. *Gondwana Res.* **2017**, *45*, 208–227. [CrossRef]

98. Mikhailenko, D.S.; Rezvukhin, D.I.; Korsakov, A.V.; Sobolev, N.V. Olivine in a coesite-bearing eclogite from the Udachnaya kimberlite pipe. *Dokl. Earth Sci.* **2019**, *489*, 1358–1362. [CrossRef]

99. Mikhailenko, D.; Golovin, A.; Korsakov, A.; Aulbach, S.; Gerdes, A.; Ragozin, A. Metasomatic evolution of coesite-bearing diamondiferous eclogite from the Udachnaya kimberlite. *Minerals* **2020**, *10*, 383. [CrossRef]

100. Misra, K.C.; Anand, M.; Taylor, L.A.; Sobolev, N.V. Multi-stage metasomatism of diamondiferous eclogite xenoliths from the Udachnaya kimberlite pipe, Yakutia, Siberia. *Contrib. Mineral. Petrol.* **2004**, *146*, 696–714. [CrossRef]

101. Spetsius, Z.V.; Taylor, L.A. Partial melting in mantle eclogite xenoliths: Connections with diamond paragenesis. *Int. Geol. Rev.* **2002**, *44*, 973–987. [CrossRef]

102. Sobolev, N.V. *Deep Seated Inclusions in Kimberlites and the Problem of the Composition of the Upper Mantle*; AGU: Washington, DC, USA, 1977; p. 304.

103. Perchuk, L.L.; Safonov, O.G.; Yapaskurt, V.O.; Barton, J.M., Jr. Crystal-melt equilibria involving potassium-bearing clinopyroxene as indicator of mantle-derived ultrahigh-potassic liquids: An analytical review. *Lithos* **2002**, *60*, 89–111. [CrossRef]

104. Enggist, A.; Chu, L.L.; Luth, R.W. Phase relations of phlogopite with magnesite from 4 to 8 GPa. *Contrib. Mineral. Petrol.* **2012**, *163*, 467–481. [CrossRef]

105. Enggist, A.; Luth, R.W. Phase relations of phlogopite and pyroxene with magnesite from 4 to 8 GPa: KCMAS–H_2O and KCMAS–H_2O–CO_2. *Contrib. Mineral. Petrol.* **2016**, *171*, 88. [CrossRef]

106. Sobolev, N.V.; Kaminsky, F.V.; Griffin, W.L.; Yefimova, E.S.; Win, T.T.; Ryan, C.G.; Botkunov, A.I. Mineral inclusions in diamonds from the Sputnik kimberlite pipe, Yakutia. *Lithos* **1997**, *39*, 135–157. [CrossRef]

107. Sobolev, N.V.; Logvinova, A.M.; Efimova, E.S. Syngenetic phlogopite inclusions in kimberlite-hosted diamonds: Implications for role of volatiles in diamond formation. *Russ. Geol. Geophys.* **2009**, *50*, 1234–1248. [CrossRef]

108. Shatsky, V.S.; Zedgenizov, D.A.; Ragozin, A.L.; Kalinina, V.V. Diamondiferous subcontinental lithospheric mantle of the northeastern Siberian Craton: Evidence from mineral inclusions in alluvial diamonds. *Gondwana Res.* **2015**, *28*, 106–120. [CrossRef]

109. Brey, G.P.; Bulatov, V.K.; Girnis, A.V.; Lahaye, Y. Experimental melting of carbonated peridotite at 6–10 GPa. *J. Petrol.* **2008**, *49*, 797–821. [CrossRef]

110. Wyllie, P.J.; Huang, W.L. Inflence of mantle CO_2 ingeneration of carbonatites and kimberlites. *Nature* **1975**, *257*, 297–299. [CrossRef]

111. Moussallam, Y.; Morizet, Y.; Massuyeau, M.; Laumonier, M.; Gaillard, F. CO_2 solubility in kimberlite melts. *Chem. Geol.* **2014**, *418*, 198–205. [CrossRef]

112. Sharygin, I.; Litasov, K.; Shatskiy, A.; Golovin, A.; Ohtani, E.; Pokhilenko, N. Melting phase relations of the Udachnaya-East group-I kimberlite at 3.0–6.5 GPa: Experimental evidence for alkali-carbonatite composition of primary kimberlite melts and implications for mantle plumes. *Gondwana Res.* **2015**, *28*, 1391–1414. [CrossRef]

113. Litasov, K.D.; Sharygin, I.S.; Shatskiy, A.F.; Ohtani, E.; Pokhilenko, N.P. Experimental constraints on the role of chloride in the origin and evolution of kimberlitic magma. *Dokl. Earth Sci.* **2010**, *435*, 1641–1646. [CrossRef]

114. Sokol, A.G.; Kupriyanov, I.N.; Palyanov, Y.N.; Kruk, A.N.; Sobolev, N.V. Melting experiments on the Udachnaya kimberlite at 6.3–7.5 GPa: Implications for the role of H_2O in magma generation and formation of hydrous olivine. *Geochim. Et Cosmochim. Acta* **2013**, *101*, 133–155. [CrossRef]